On the importance of phenology in the Miombo ecosystem:

Evaluation of open-source satellite evaporation models

*Henry Zimba[1'2], Miriam Coenders-Gerrits[1], Kawawa Banda[3], Petra Hulsman[4], Nick van de Giesen[1], Imasiku Nyambe[3], Hubert. H. G. Savenije[1].

5 [1] Delft University of Technology, Water Resources Section, Building 23 (Faculty of Civil Engineering and Geosciences) 2628 CN Delft, P.O Box 5048 2600 GA Delft, The Netherlands.

[2] Ministry of Agriculture, Department of Agriculture, P.O Box 50595, Mulungushi House, Independence Avenue, Lusaka, Zambia.

[3] University of Zambia, Integrated Water Resources Management Centre, Department of Geology, School of
10 Mines, Great East Road Campus, Lusaka, Zambia.

[4] Ghent University, Hydro-Climate Extremes Lab (H-CEL), Coupure links 653, 9000 Ghent, Belgium

*Corresponding author: h.m.zimba@tudelft.nl

15 **Abstract**

Accurate spatial-temporal information on evaporation is needed for use in many sectors including hydrology, agriculture and climate studies. This would require a dense observation network, which is practically impossible. Over the past decades, remotely sensed evaporation models to estimate spatially continuous evaporation have been developed. However, deciding which model to use is a challenge as these models vary in complexity and accuracy
20 across the different global ecosystems. It is even more challenging for complex African ecosystems that have very few, or none at all, flux tower observations. In this study, we used the general water balance evaporation (E_{wb}) as reference to which we compared six models that determine evaporation, i.e., $FLEX-Topo_{WB}$, TerraClimate (TMC_{WB}), GLEAM, MOD16, SSEBop and WaPOR, in the Luangwa Basin, a semi-arid catchment in the Miombo ecosystem in southern Africa. $FLEX-Topo_{WB}$ and TMC_{WB} models are calibrated on discharge, while GLEAM,
25 MOD16, SSEBop and WaPOR have been validated on evaporation data from flux tower observations. Key focus is on inter-model performance comparison in the Miombo ecosystem across phenophases and land cover types. Results show that major spatial-temporal discrepancies in model performance occur in the forest and open water body land surfaces during the dormant and green-up phenophases in the dry season. Compared to E_{wb}, annually WaPOR consistently overestimated evaporation while GLEAM consistently underestimated evaporation. The rest
30 of the models showed biases within the GLEAM and WaPOR boundaries. With reference to annual mean bias SSEBop and WaPOR showed lowest aggregated 2009 -2020 bias in terms of estimating long-term average annual evaporation. It appears that correct understanding of the Miombo vegetation phenology associated moisture feedbacks and incorporating these in model structure is likely to improve evaporation estimates in the Luangwa Basin and Miombo Woodland ecosystem as a whole.

1.0   Introduction

35   Miralles et al. (2020) defines evaporation as "the phenomenon by which a substance is converted from its liquid into its vapour phase, independently of where it lies in nature". Instead of the often-used term 'evapotranspiration', in this paper we use the term evaporation for all forms of terrestrial evaporation, including transpiration by leaves, evaporation from intercepted rainfall by vegetation and forest floor, soil evaporation, and

40   evaporation from stagnant open water and pools (Miralles et al., 2020; Savenije 2004). Estimates indicate that through the evaporation process, the land surface transfers about 60 per cent of precipitation back to the atmosphere (Oki and Kanae, 2006; Van der Ent et al., 2010). Evaporation, through latent heat transfer, also helps in understanding the energy partitioning at the earth's surface (Trenberth et al., 2009; Fisher et al., 2008). Therefore, evaporation is considered a significant factor in the recycling of water available at the land surface (Van der Ent

45   et al. 2010; Oki and Kanae, 2006). As a result, accurate estimation of evaporation is important as this allows for an improved and deepened understanding of water and energy cycles. However, ascertaining evaporation using field observations is a tedious, complex and expensive requiring specific devices and accurate measurements of various physical variables at different time intervals and spatial scales (Jiménez-Rodríguez et al., 2021; Coenders-Gerrits et al., 2020; Gerrits et al., 2007; Dyck, 1972). The field observations, which are normally point-based, are

50   limited in application due to the shortcomings in the temporal and spatial scale. Furthermore, heterogeneity in the land surface and the loss of high accuracy of the measured values when upscaling to larger regions also limits its application (Dyck, 1972). Currently, assessment of evaporation is mainly from site observations at point scale using various approaches including, eddy covariance (Foken, Aubinet, and Leuning, 2012), lysimeters (Trajkovic, 2010) and the Bowen ratio energy balance (Lakhiar et al., 2018; Schilperoort et al., 2018; Spittlehouse and Black,

55   1980; Bowen, 1926). To bridge these gaps there has been accelerated development and application of satellite-based approaches to estimate evaporation at local, regional and global scales. Thus, evaporation estimates based on satellite data, ~~largely,~~ are bridging the gaps associated with field data collection, i.e., spatial and temporal constraints (McCabe, 2019; Zhang et al., 2016; Kalma et al., 2008; McCabe and Wood, 2006).

Despite availability of several open-~~source~~ satellite evaporation models (i.e. Martens et al., 2017; Zhang

60   et al., 2016; Miralles et al., 2011; Mu et al., 2011; Savoca et al., 2013; Bastiaanssen et al., 1998) these models differ in the spatial-temporal estimation of evaporation across land surfaces and scales (Weerasinghe et al 2020; Jiménez et al., 2011; McCabe & Wood, 2006). Additionally, no consensus exists on which of these models is best taking into account each has its advantages and disadvantages depending on application (Zhang et al., 2016). To explore the relative merits of these models some studies have been done at global and African continent scales

65   (i.e., Blatchford et al., 2020; Dile et al., 2020; Weerasinghe et al., 2020; Jiménez et al., 2011; Miralles et al., 2016; Liu et al., 2016). The overall outcome of these studies is that the accuracy of model estimates is land surface or ecosystem dependent and it varies among ecosystems globally. Furthermore, these remote sensing evaporation models are validated only on locations where in-situ observations exists. For the African continent, in-situ observations are extremely sparse and limited temporally. Additionally, African ecosystems are uniquely diverse

70   and thus it is questionable whether performance of evaporation models is valid for these ecosystems.

Evaluation of models in non-Miombo ecosystems in Africa is not representative for evaporation model behaviour in the Miombo Woodland. Furthermore, for Africa, Weerasinghe et al. (2020) recommended that at catchment scale detailed assessment of models performance be conducted taking into account the characteristics of the specific basin. There is a need to evaluate performance of evaporation models specifically for the Miombo

75   Woodland basins. This is because the Miombo Woodland is Africa's largest tropical seasonal woodland and is a
dry forest formation that forms a transition zone between tropical rainforest and the African Savannah across 11
countries. It is an extremely important ecosystem in the food, water and energy nexus of Southern Africa (Gumbo
et al., 2018; Chidumayo & Gumbo, 2010; Frost, 1996). The Miombo Woodland is also a significant carbon sink
crucial in climate change mitigation (Pelletier et al. 2018). Also, noteworthy is the plant species diversity that

80   defines the Miombo ecosystem across its spatial vastness (Gonçalves et al., 2017; Giliba et al., 2011; Mapaure,
2001; Frost, 1996; Chidumayo, 1987). Different plant species have varying biophysical attributes and interacts
differently with the hydrological cycle. In the context of the vast Miombo ecosystem, this implies that species
composition in a given basin influences the evaporation characteristics of that basin. This means that actual
evaporation patterns at regional or basin scale are simply a summation of compartmentalized local forest and sub

85   basin actual evaporation patterns. Therefore, understanding the evaporation pattern at various scales in the Miombo
ecosystem is essential to understanding the overall characteristic of the evaporation dynamics at the ecosystem
level. Both Pelletier et al. (2018) and Tian et al. (2018) postulated that the functional traits of the Miombo
Woodlands vegetation species is different from other ecosystems. By implication, the dissimilarities in the
Miombo Woodland's ecological processes with other ecosystems in Africa signals the possibility of unique

90   evaporation models behaviour in this complex ecosystem. Furthermore, these evaporation models are normally
structured for agricultural purposes. However, crop plant moisture feedbacks are different from natural vegetation
as they have different physiological attributes and interact differently with changing hydrological regimes. Of the
few evaluation studies done in Africa (i.e., Blatchford et al., 2020; Dile et al., 2020; Weerasinghe et al., 2020),
those that included a Miombo Woodlands basin used global scale water balance as reference data. Furthermore,

95   the studies did not focus on the potential influence of Miombo Woodland phenological dynamics and plant-water
interaction influence on models' performance across seasons. However, what is common are the findings of these
studies that satellite-based evaporation products have a mixed performance across the African ecosystems, as they
tend to either overestimate or underestimate evaporation. They attribute this behaviour mainly to the uncertainties
associated with model structure, forcing data, model processes and scaling (Pagán et al., 2019).

100   In the context of the Miombo ecosystem region, making a choice on which open-source evaporation
model to use is extremely difficult due to extremely limited ecosystem specific validation studies. This constraint
is attributed to very few fluxes observation sites in the region. However, in absence of spatially distributed field
evaporation observations, it is still possible to assess model performance at catchment level using the general water
balance approach (precipitation minus surface runoff) (i.e., Weerasinghe et al., 2020; Liu et al., 2016).

105   We formulated this study to contribute to bridging the gap in information on satellite-based evaporation
models performance in the Miombo ecosystem. Focus was on the Luangwa sub-basin in the larger Zambezi Basin,
one of the largest river basins in the Miombo ecosystem. We chose the Luangwa Basin because it is located in a
sparsely gauged semi-arid region (Beilfuss, 2012) where management of water resources, based on reliable
information, for various competing uses i.e. hydropower, agriculture, wildlife, industrial and domestic (WARMA,

110   2022) is essential. The Luangwa Basin also falls within two of the largest Miombo Woodland sub-groups: dry
southern Miombo Woodlands and wet central Zambezian Miombo Woodlands. The central Zambezian Miombo
is the largest of the four Miombo sub-groups the other three being the Angolan Miombo, Eastern Miombo, and
the Southern Miombo (Frost, 1996; White, 1984). It is also located in Zambia, argued to have the highest diversity
of Miombo Woodland trees and considered centre of endemism for the Miombo Woodlands Brachystegia species

115   (Frost, 1996). These attributes suggest a catchment that is a fair representation of the Miombo Woodlands conditions and an appropriate site for this type of study. Therefore, our aim was twofold:

1) Compare performance of six open access and commonly used evaporation models at sub-basin level against the general water balance approach in the Luangwa Basin. Focus was to observe models' performance in relation to phenological transitions and land cover types.

120   2) We discuss potential underlying factors that could be contributing to the observed discrepancies in models' behaviour.

2.0   Materials and Methods

2.1   Study approach

The model performance comparison was done at monthly, seasonal and annual temporal scales. At annual

125   scale we compared six evaporation models to the general water balance evaporation (E_{wb}) for the period 2009 - 2020. We deemed the 12 year period sufficient to capture long-term seasonal, monthly and annual variations in catchment evaporation. At monthly scale, we intercompared the performance of the six models with focus on the rain and dry seasons and the various phenophases in the Luangwa Basin. The six models included $FLEX - Topo_{WB}$ (Hulsman et al., 2021; Hulsman et al., 2020; Savenije, 2010), TerraClimate Thornthwaite-

130   Mather Climatic water balance model (TMC_{WB}) (Abatzoglou et al., 2018) and Global Land Evaporation Amsterdam Model (GLEAM) (Martens et al., 2017; Miralles et al., 2011). The others are the Moderate-resolution Imaging Spectrometer (MODIS) MOD16 (Running et al., 2019; Mu et al., 2011; Mu et al., 2007), Operational Simplified Surface Energy Balance (SSEBop) (Savoca et al., 2013) and the Water Productivity through Open access of Remotely sensed derived data (WaPOR)(FAO 2018). In the absence of field observation of evaporation

135   we chose $FLEX - Topo_{WB}$ and TMC_{WB} as reference evaporation at monthly scale because they are calibrated on observed discharge and not on Eddy Covariance tower data from locations outside the Miombo region and Luangwa Basin specifically. We selected GLEAM, MOD16, SSEBop and WaPOR because they are open source with both historical and real-time data. Additionally, they have desirable spatial-temporal attributes for monitoring evaporation and are commonly used products globally with WaPOR being a continental product.

140   Compared to other ecosystems, Pelletier et al. (2018) and Tian et al. (2018) observed that Miombo Woodland species exhibit distinct behaviour during the dry season. In view of Pelletier et al. (2018) and Tian et al. (2018) observations, we ascertained existence of discrepancies in spatial-temporal model performance that reflect the distinct behaviour under changing seasons (i.e., dry (May - October) and wet (October – April) seasons) and phenological stages of the Miombo Woodland and Luangwa Basin in general. We compared model

145   performance during seven Miombo Woodland phenophases. We based the phenophases classification on the Collection 6 MODIS Land Cover Dynamics (MCD12Q2) Product (Gray et al., 2019), Zimba et al. (2020), as well as on own field observations of the Miombo phenology in the Luangwa Basin. Figure 1 highlights the phenophases classification. The phenophases include; Green-up, Mid-Green up, Maturity, Peak, Senescence, Green-down, and Mid-green down and dormant. For easy of analysis we merged the phenophases into four groups (Figure 1) based

150   on dominant activity in each phase.
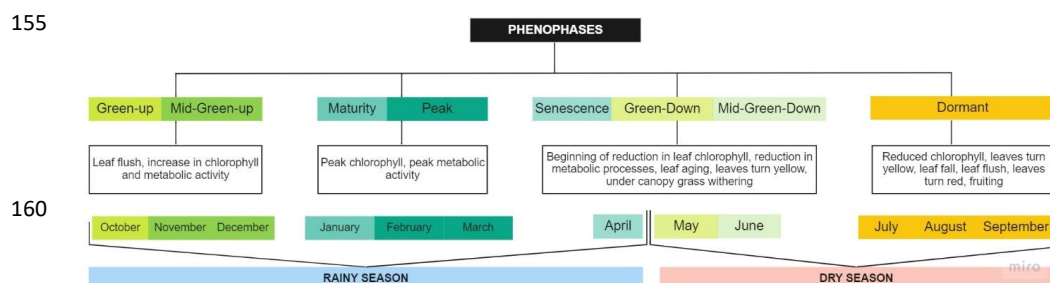
Figure 1. Grouping and description of phenophases in relation to seasonality for the Luangwa Basin used in the study.

The water balance evaporation (E_{wb}) has been estimated using equation 1 where we neglect storage change over a year.

$$E_{wb} = P - Q \qquad (1)$$

Where, P is the catchment precipitation in mm/year and Q is discharge/catchment surface runoff in mm/year. Oki and Kanae (2006) and Zhang et al. (2016) indicated that model inputs are one of the major sources of uncertainties in evaporation model performance. For rainfall and discharge, we made use of the TerraClimate product, which we validated with local observations. In Appendix Figure A1.1, we show the comparison between TerraClimate and observed discharge records. For the simulations the regression between observed and TerraClimate was used to extend the period of observations from 2009 - 2020. For the precipitation we conducted a validation exercise on three precipitation products which included the Climate Hazards Group InfraRed Precipitation with Station data (CHIRPS), Climate Forecast System Reanalysis (CFSR) and TerraClimate precipitation. The assessment was done at monthly and annual scales for years with complete field observations. The field data was obtained from the SASSCAL WeatherNet at Kabwe and Serenje weather ststaions (http://www.sasscalweathernet.org) and the ZAMSECUR project field observations (Mpika station). Location of the weather stations is shown in Figure 2. The Kabwe and Serenje stations had complete data sets for the period 2014-2016 and Mpika 2020 -2021. The TerraClimate precipitation product appeard to have the least bias for the E_{wb} reference evaporation. After validating precipitation, we assessed monotonic trends in long-term (2009 – 2020) mean monthly and annual evaporation datasets (i.e., Weerasinghe et al., 2020; Liu et al., 2016).

Different land surfaces, i.e., forests, grassland, open water body give different evaporation feedbacks (Granger and Hedstrom, 2010; Moors, 2012; Makkink, 1957). To this extent, we compared model performances based on six major land cover types; dense forest, mixed open forest and grassland, shrub-land, cropland, open water body and build up area. We used monthly evaporation averages for the period 2009 – 2020. The six land cover classes were purposively selected based on verified field observations of the land cover done between 2018 and 2021 in the Luangwa Basin. We selected areas with minimal potential for land cover class transitioning into other classes overtime. For instance, the dense forest land cover was based on a protected natural forest in a conservancy region, irrigated crop land cover was based on known established active commercial farmlands that have been in existent for over ten years. Rain-fed cropland was selected from areas with established rural

195   settlements and cropland. Build up area/settlement was based on an old and expanding urban settlement. Shrub-
land was selected from a game reserve area. To augment the correct selection of the land-cover types we used high
resolution google earth platform. We compared the field based land cover data points with the Copernicus 2019
land cover classification for the Luangwa Basin. The Copernicus land cover product uses high spatial-resolution
(10 m) Sentinel data for classification with more detail than other products. Special focus was on the comparison

200   of models in the dense forest across the phenophases.

To observe changes in canopy display in Miombo forest we installed a Denver digital camera on a tower
above the canopy of a known Miombo forest in Mpika (Figure 2). This was done to obtain field imagery to compare
with the pattern of satellite-based normalised difference vegetation index (NDVI) and evaporation model
behaviour at different stages of the canopy display pattern. The observations were done for the period January –

205   December 2021.

To establish relationships among variables and assessing accuracy of models we used various statistical
models. We checked for monotonic trends and coupled magnitude in evaporation time series using non-parametric
Mann-Kendall (Helsel et al., 2020) trends test (equation A1-A6 in section A1.1 in the appendices). We tested for
trends at monthly and annual temporal scales for the period 2009 - 2020. To establish correlation among the models

210   the Kendall correlation test (Helsel et al., 2020; Kendall, 1975) (equations A7 in section A1.2 in the appendices)
was used. Correlation was assessed at monthly and annual scales. Model performance assessment was done using
the coefficient of determination (R^2) (Helsel et al., 2020) (equation A8 in section A1.3 in the appendices), root
mean square error (RMSE) (Helsel et al., 2020) (equation A9 in section A1.3 in the appendices) and the mean bias
(Helsel et al., 2020) (equation 2).

215   The mean Bias is the measure of the extent to which modelled values deviate from observed values. It
indicates whether there is under or overestimation of values by the model. The interpretation is that the smaller the
mean Bias value (positive or negative) the less the deviation of the predicted values from the observed values.

$$Mean \text{ Bias} = \sum(X - \hat{Y})/N \tag{2}$$

220   Where N = number of observations, Y = actual observations time series and X is the modelled time series.
Statistical analyses were done for the annual scale, rain and dry seasons and for phenophases.

2.2   Study site

The Luangwa is a sub-basin in the larger Zambezi Basin in sub-Saharan Africa in Zambia (Figure 2). It
is about 159,000 km^2 in spatial extent and is largely covered with deciduous forests, herbaceous wetlands, shrubs

225   and herbaceous vegetation/savanna (Figure 2; Phiri et al. (2019)). Elevation ranges between 318 – 2327 m above
mean sea level with the central part generally a valley (Figure 2). The Luangwa River, 770 km long, and its
tributaries drain the basin (Beilfuss 2012). The Luangwa Basin is scarcely gauged and with paucity of data on
various hydrological aspects. The basin is located in a semi-arid environment characterised by a well-delineated
wet season, from October to April and a dry season, May to October. Furthermore, the dry season is split into the

230   cool-dry (May to August) and hot dry (August to October) seasons. The movements of the inter-tropical
convergence zone (ITCZ) over Zambia between October and April dominate the rainfall activity in the basin. The
basin has a mean annual precipitation of about 970 mm.yr^{-1}, potential evaporation of about 1560 mm.
yr^{-1}, and river runoff reaches about 100 mm.yr^{-1} (Beilfuss, 2012; World Bank, 2010). The key character of

the deciduous forests is that they shed off old leaves and acquire new ones during the period May to October in
235   the dry season. Frost (1996) revealed that depending on the amounts of rainfall received in the preceding rain
season the leaf fall and leaf flush processes may start early (i.e., in case of low rainfall received) or late (in case of
high rainfall received) and may go up to November (i.e., in the case of high rainfall received).
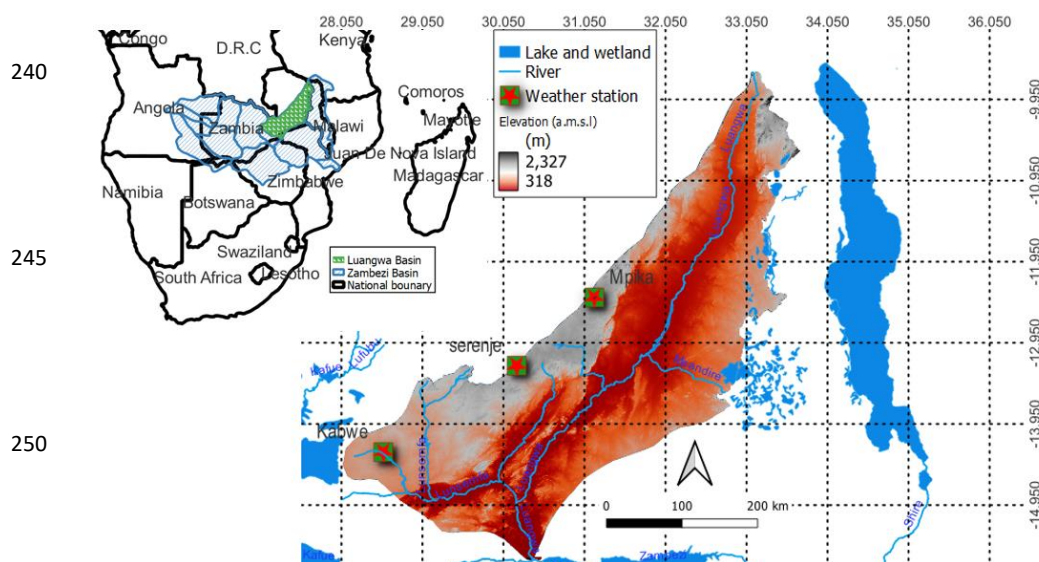
255   Figure 2. Location of the Luangwa Basin in the Zambezi Basin in Zambia and spatial distribution of elevation with
ASTER digital elevation model.

According to Phiri et al. (2019), the basin is largely covered by primary and secondary deciduous forests.
Primary forests are parcels of forests without anthropogenic disturbances while secondary forests are
260   characteristically regenerated forests after anthropogenic disturbances. The larger component of the forest in the
basin seems to fall under the secondary forest. This is indicative of increased anthropogenic activities such as
commercial and small-holder agriculture in the basin. Another anthropogenic activity that affects Miombo forest
and the general Luangwa Basin landscape are the wide spread annual wild fires, which result in large areas getting
burnt. The fires normally occur between May and November in the dry season (Phiri et al., 2019; Frost,1996). The
265   Luangwa Basin also hosts hydro-power stations located on tributaries (i.e., Lunsemfwa River) to the Luangwa
River (Phiri et al., 2019).

2.3   Meteorological conditions during study period

Figure 3 shows the spatial (A-D) and temporal (E-H) distribution of average precipitation, temperature, soil
270   moisture and net radiation for the study area during the period 2009 – 2020. From Figure 3A we see that the
highlands receive more rainfall than the low lands. In terms of the temporal distribution (Figure 3E), much of the
precipitation is between December and April. Across the basin, spatial distribution of temperature (Figure 3 B&F)
varied with lower temperatures observed in high soil moisture content (Figure 3 C & G), high rainfall temperature

environments. Like with the air temperature, monthly net radiation (Figure 3 D & H) spatially varies across the

275   basin ranging between 100 - 200 W.m⁻². High net radiation, of above 150 W.m⁻², is observed for period September

- February. Net radiation is lowest during the cool dry season, May - August.
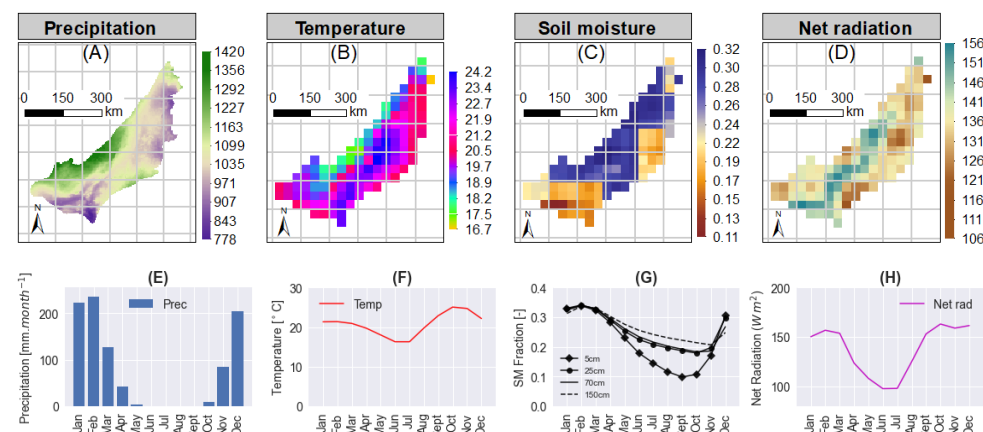
Figure 3. (A-D) Spatial distribution of long-term (2009 -2020) TerraClimate precipitation (mm/year) and CFSR

soil moisture (m³.m⁻³), air temperature (°C) and net radiation (W.m⁻²) in the Luangwa Basin. (E-H) Long-term

(2009 – 2020) averages showing the monthly temporal distribution of precipitation, soil moisture, air temperature

and net radiation for the Luangwa Basin.

290

2.4   Data sets

~~Apart from the~~ E_{wb}, we used six evaporation products that included two water balance evaporation

models (WBM) FLEX-Topo$_{WB}$ and TMC_{WB} and four energy balance evaporation models (EBM) GLEAM,

MOD16, SSEBop and WaPOR (Table 1).

295   We used the FLEX-Topo$_{WB}$ because it was structured specifically for the Luangwa Basin landscape and

was calibrated on field observations-based discharge of the basin at a daily temporal scale (Hulsman et al., 2021).

We forced FLEX-Topo$_{WB}$ model with spatially distributed CHIRPS precipitation and GLEAM potential

evaporation. Each cell has been discretised into functionally distinct hydrological response units (HRU) based on

the topography. The model uses a single ground water system within a grid cell to which all HRU are connected.

300   It is composed of several storage components representing the interception storage, unsaturated root-zone storage,

as well as fast and slow responding storages. Furthermore, each storage component has been structured as a

reservoir with matching water balance equations. In terms of performance, with respect to observed discharge,

calibrated for the period 2004 -2009, the model performed relatively well with the following Nash-Sutcliffe metric;

NS_Q = 0.66 (using discharge time-series), NS_log (Q) = 0.82 (using logarithmic discharge time-series), NS_FDC

305   = 0.91 (using flow duration curve) and NS_log (FDC) = 0.97 (using logarithmic flow duration curve). However,

the limitation with the FLEX-Topo$_{WB}$ was the 27.7 km spatial resolution. Compared to FLEX-Topo$_{WB,}$ TMC_{WB} is

a relatively high spatial resolution water balance product. Like FLEX-Topo$_{WB}$, it is also calibrated with field

observations based on the Global Runoff Data Centre (GRDC) data set (Abatzoglou et al., 2018). It has shown

good results in ecosystems where it has been validated and compared relatively well with other evaporation

310   products (Abatzoglou et al., 2018). In our study, calibration with basin discharge, the 4 km spatial resolution and monthly temporal resolution were desirable attributes for use as reference evaporation.

As evaporation products, GLEAM, MOD16, SSEBop and WaPOR were selected for use in this study because they are open -source products with wide usage across Africa and the globe in the case of GLEAM, MOD16 and SSEBop. Except GLEAM (with spatial resolution of 27.7 km), these products have high spatial
315   resolution (i.e., 500m, 1000m and 250 m for MOD16, SSEBop and WaPOR respectively) and temporal resolution (daily, 8-day and decadal respectively) which are attributes suitable for our application. GLEAM and WaPOR account for interception and vegetation interaction with the root zone storage. These are important aspects in the evaporation processes and potentially significant components in the Miombo ecosystem evaporation. Since different land cover surfaces have different moisture feedbacks, the use of land cover products in GLEAM,
320   MOD16 and WaPOR are likely to give better representation of spatial distribution of moisture feedbacks in the Miombo ecosystem. It is an established fact that different land surfaces have specific land surface temperature feedbacks (i.e., Rocha et al., 2020; Sun et al., 2016) a principal utilised by SSEBop model to estimate evaporation. Since the Miombo ecosystem and the Luangwa Basin in particular is a water limited semi-arid environment the use of the land surface temperature feedbacks to estimate evaporation could prove a more reliable approach in this
325   ecosystem. In general, we selected these evaporation products based on the potential of the structure and processes to capture moisture feedbacks in a unique ecosystem in a semi-arid environment.

Table 1. Characteristics of data used in this study

Variable	Product name	Time Period	Spatial coverage/Location	Temporal resolution	Spatial resolution	Reference	Source of data
Precipitation and temperature	CFSR v2	2014 - 2020	Global	Daily	19.2 km	(Saha et al. 2014; Saha et al. 2010)	Climate Engine
	CHIRPS	2014 - 2020	Global	Daily	N/A	(Funk et al., 2015)	Climate Engine
	Observation (Mpika)	2020 - 2021	Point (-12.385063, 31.171189)	Daily	N/A	N/A	https://doi.org/10.4121/19372352.v2
	Observation (Kabwe)	2014-2017	Point(-13.226700, 30.215080)	Daily	N/A	N/A	http://www.sasscalweathernet.org
	Observation (Serenje)	2014-2017	Point(-14.291745, 28.567684)	Daily	N/A	N/A	http://www.sasscalweathernet.org
Land surface temperature	TerraClimate	2009 - 2020	Global	Monthly	5 km	(Abatzoglou et al. 2018)	Climate Engine
	MOD11A2 and MYD11A2	2020	Global	8-day	1 km	(Wan et al., 2015)	Climate Engine
NDVI	MODIS	2009-2020	Global	16-days	0.5 km	(Didan 2015)	Climate Engine
Burnt area	MODIS	2020	Global	Daily	0.5 km	(Giglio et al., 2015)	Climate Engine
Runoff	Observations	1981-1990	N/A	Daily	N/A		WARMA, Zambia
	TerraClimate	2009 - 2020	Global	Monthly	5 km	(Abatzoglou et al. 2018)	Climate Engine
Net radiation	CFSR v2	2009-2020	Global	Daily	19.2 km	(Saha et al. 2014; Saha et al. 2010)	Climate Engine
Soil moisture	CFSR v2	2009-2020	Global	Daily	19.2 km	(Saha et al. 2014; Saha et al. 2010)	Climate Engine
Digital elevation model (DEM)	ASTER GDEM v3	N/A	Global	N/A	30	(Abrams and Crippen, 2019)	NASA Glovis portal
Land cover map	Copernicus CGLS-LC100 v3	2019	Global	Annual	100	(Smets Bert De Roo, 2020)	Google Earth Engine
Evaporation	FLEX-Topo$_{WB}$	2009 - 2020	Catchment	Daily	27.7 km	(Hulsman et al., 2021; Hulsman et al., 2020; Savenije, 2010)	This study
	GLEAM (v3.2a)	2009 -2020	Global	Daily	27.7 km	(Martens et al., 2017; Miralles et al., 2011)	GLEAM FTP server
	MOD16v2	2009 -2020	Global	8-day	0.5 km	(Running et al., 2019; Mu et al., 2011)	Global subsets tool: MODIS/VIIRS Land Products
	SSEBop	2009 -2020	Global	Monthly	1 km	(Savoca et al., 2013).	Climate engine
	TMC_{WB}	2009 -2020	Global	Monthly	4 km	(Abatzoglou et al. 2018)	Climate engine
	WaPOR v2. (ETLook)	2009 -2020	Continental	Decadal	0.25 km	("WaPOR Database Methodol.," 2020; FAO, 2018)	WaPOR Portal

330 **3.0   Results**

3.1   Sensitivity of precipitation products and trends analysis of evaporation products

Figure A1 in the appendices shows the validation results of the precipitation products. Overall, the
TerraClimate precipitation showed the least bias and was thus used in the general water balance evaporation
estimates. Figure A2 in the appendices shows the results of the comparison of TerraClimate runoff data with field
335 observations and regression results. The regression results are close to field observations hence the use of the
approach to extend runoff estimates for the period 2009-2020. Table 2 and Table A2 (in the appendices) shows
annual and monthly descriptive and Mann-Kendall trends analysis statics for the various evaporation products
used in the study. At both monthly and annual scales, except for the SSEBop with a significant monthly seasonal
downward trend (Table A1 in the appendices), all other evaporation products showed no significant trend in
340 evaporation as the computed Z-test statistics were $-1.96 < Z(c) < 1.96$ and the p-values were greater than the alpha
level 0.05. The non-existent of significant trend in long-term basin evaporation fulfilled the condition for use of
the general water balance to estimate basin-scale reference evaporation for comparison across different times. At
annual scale, except for the E_{wb} (14 percent), the rest of the evaporation products showed less than 10 percent
annual variation in evaporation estimates. However, seasonal monthly evaporation showed variations of up to 60
345 percent (i.e., TMC_{WB} and MOD16) (Table A1 in the appendices). The large variability when a wet year follows a
dry year, or vise-versa (as we see between 2014 and 2017 in Figure 4), is due to over-year storage that the water
balance methods neglects at annual scale.

Table 2. Descriptive and Mann-Kendall trends statics for each model for the period 2009 - 2020

Statistic	No	Min	Max	Mean	SD	VC	Z-test	β	p-value	Alpha	Decision
TMC_{WB}.	12	694.87	940.68	808.26	79.01	0.09	0.07	1.37	0.95	0.05	No trend
FLEX-Topo$_{WB}$	12	741.57	870.14	801.77	40.79	0.05	-1.44	-7.70	0.15	0.05	No trend
WaPOR	12	854.61	1039.35	970.78	50.40	0.05	-1.30	-4.46	0.19	0.05	No trend
SSEBop	12	766.94	919.14	836.91	46.40	0.05	-0.75	-5.70	0.45	0.05	No trend
GLEAM	12	656.19	772.66	721.44	34.72	0.05	-1.03	-3.12	0.30	0.05	No trend
MOD16	12	756.16	861.79	806.96	31.55	0.04	0.34	0.68	0.73	0.05	No trend
E_{wb}	12	644.19	1070.70	821.01	122.72	0.14	0.21	5.10	0.84	0.05	No trend

350 **Interpretation:** *No. = number of observation, Min = minimum, Max = maximum, SD = standard deviation, VC = variation coefficient*

3.2   Temporal variability in evaporation and model performance at annual scale

Figure 4A shows the annual evaporation and TerraClimate precipitation while Figure 4B gives the annual
Bias for each model with reference to E_{wb} for the period 2009 – 2020. Figure A3 in the appendices shows
355 performance statics of the models at annual scale. As mentioned above, the peak and dip in the bias in the period
2014 – 2017 is an artefact of the general water balance method that neglects over-year storage. Across the
examined period, annual estimates of evaporation varied from model to model with the WaPOR and GLEAM at
the upper and lower end respectively. It appeared, that except for TMC_{WB}, the rest of the models did not
consistently respond appropriately to changes in annual precipitation. With reference to E_{wb}, compared to other
360 EBM the WaPOR consistently overestimated annual evaporation and GLEAM consistently underestimated annual
evaporation. Between 2009 and 2014, $FLEX - Topo_{WB}, TMC_{WB}$, MOD16 and SSEBop evaporation pattern
aligned relatively well with low biases. However, between 2015 and 2020 TMC_{WB} showed higher evaporation
estimates than the $FLEX - Topo_{WB}$, MOD16 and SSEBop but followed E_{wb} pattern (Figure 4).
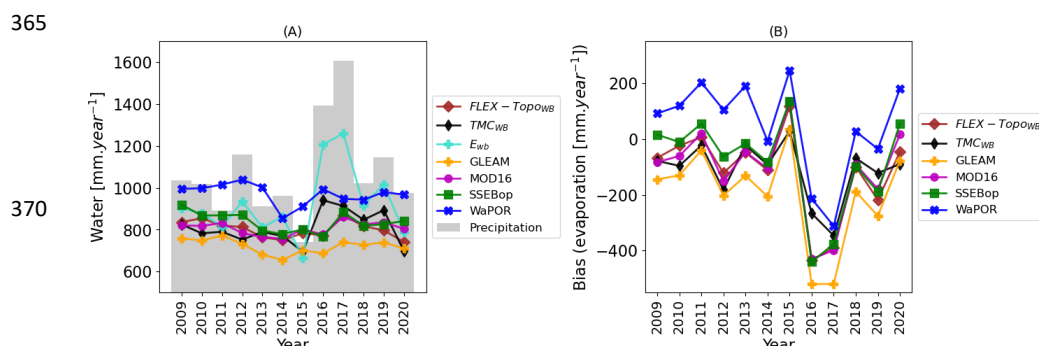
Figure 4. (A) EBM and WBM temporal pattern of average annual evaporation and (B) annual bias evaporation of models with reference to the general water balance (E_{wb}) for the period 2009 – 2020 in the Luangwa Basin.

There is weak correlation (r < 0.4) between $FLEX - Topo_{WB}$ and TMC_{WB} (Table A2 in the appendices). Except with the WaPOR, $FLEX - Topo_{WB}$ exhibited strong (r > 0.7) annual correlation with GLEAM, MOD16 and SSEBop. E_{wb} and TMC_{WB} showed weak (r< 0.4) correlation with all EBM (Table A2 in the appendices). With reference to the E_{wb} (Figure 4B), except for the years 2016, 2017 and 2019 WaPOR overestimated evaporation and showed a bias range of -311 to 245.34 mm.year^{-1}. The rest of the models generally underestimated annual evaporation with bias ranges of -434.05 to 117.7 mm.year^{-1} for $FLEX - Topo_{WB}$, -346 to 28.70 mm.year^{-1} for TMC_{WB}, -519.59 to 35.34 mm.year^{-1} for GLEAM, -430.05 to 16.86 mm.year^{-1} for MOD16 and -430 to 135 mm.year^{-1} for SSEBop (Figure 4B and Figure A3 in the appendices). Generally, with reference to E_{wb}, the SSEBop, MOD16 and $FLEX - Topo_{WB}$ appeared to have relatively lower annual biases compared to other models especially for the period 2009 – 2015. During the 2016 – 2020 period, the WaPOR appeared similar with other models and showed relatively lower bias (Figure 4B). For the entire 12 year period (2009 – 2020) the WaPOR showed the least aggregated mean bias of about 50 mm.year^{-1} (overestimation) followed by the SSEBop with about -84 mm.year^{-1} (underestimation). GLEAM showed the largest aggregated bias of about -200 mm.year^{-1} (underestimation) (Figure A4 in the appendices).

3.3 Temporal distribution of mean monthly evaporation, correlation and model performance

Figure 5A shows inter-annual variability in EBM and WBM monthly evaporation. Across the 2009 – 2020 period, the general pattern in the temporal distribution of evaporation for each model appeared consistent. Major discrepancies in temporal pattern appear to be seasonal with a clear distinction between the rain and dry seasons. Figure 5 B shows long-term (2009 – 2020) aggregated temporal distribution of mean monthly evaporation for EBM and WBM. The WBM and EBM models behaviour appear to agree better during the high moisture and high canopy cover period in the rainy season between November and April. Model behaviour begins to differ at the wet (October –December) and dry (March-May) season boundaries. Significant differences in model behaviour is exhibited during the dry period of the year between May and October.
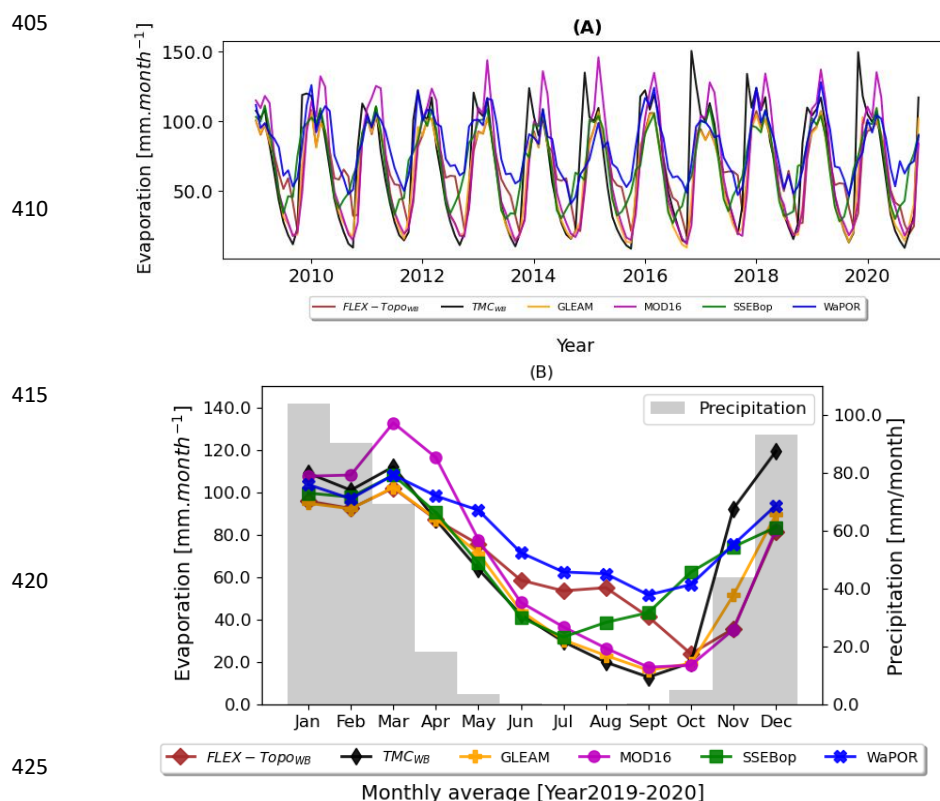
Figure 5. Comparison of models temporal distribution of mean monthly evaporation: (A) inter-annual temporal variations in mean monthly evaporation (B) Aggregated mean monthly evaporation for the rain and dry seasons in the Luangwa Basin (2009 – 2020).

Overall, during the rainy season the TMC$_{WB}$ model generally exhibit slightly higher values of evaporation compared to the other models. Reference to the FLEX-Topo$_{WB}$, EBMs, with an exception of the WaPOR and SSEBop, exhibits relatively lower evaporation estimates during the drier part of the year and the patterns also differ. Though WaPOR shows a similar temporal distribution pattern with $FLEX - Topo_{WB}$, its evaporation estimates are higher.

Subjecting the 2009 – 2020 monthly time series to a normality test showed the data was not normally distributed which necessitated the use of the non-parametric Kendall correlation test. $FLEX - Topo_{WB}$ and TMC$_{WB}$ showed similar correlation coefficients with EBM with Kendall $\tau > 0.54 \leq 0.80$ (Figure A5 and Table A3 in the appendices). $FLEX - Topo_{WB}$ had strongest correlation with GLEAM ($\tau = 0.77$), followed by MOD16 ($\tau = 0.75$), WaPOR ($\tau = 0.66$) and SSEBop ($\tau = 0.54$). TMC$_{WB}$ had strongest correlation with GLEAM ($\tau = 0.73$), followed by WaPOR ($\tau = 0.62$), MOD16 ($\tau = 0.61$) and SSEBop ($\tau = 0.54$). Intercomparison among EBM showed highest correlation ($\tau = 0.80$) was between GLEAM and MOD16 while lowest correlation ($\tau = 0.56$) was between SSEBop and WaPOR. Figure 6 shows EBM performance statistics with reference to FLEX-Topo$_{WB}$ and TMC$_{WB}$. With reference to FLEX-Topo$_{WB}$ strongest agreement with all EBMs was at the end of rain season during

445   senescence, green-down and Mid-green-down phenophases with R^2 range of 0.77 – 0.98 and Bias range 6.13 –
13.41 mm.month[-1]. The most disagreement of the EBM's with FLEX-Topo$_{WB}$ was during the dormancy
phenophase in the dry season with R^2 range 0.001 – 0.54 and Bias 8.59 - 26.75 mm.month[-1]. GLEAM, except
during Green-up and Mid-green-up, generally underestimated evaporation while WaPOR generally overestimated
evaporation across phenophases. MOD16 and SSEBop showed mixed performance with general underestimation

450   of evaporation during senescence, green-down, Mid-green down and dormant phenophases (Figure 6). With
reference to TMC$_{WB}$, like with FLEX-Topo$_{WB}$, strongest agreement with all EBM's was during senescence and
Mid-green-down phenophases with R^2 range 0.61 – 0.85 and Bias range 1.67- 22.75 mm.month[-1]. The most
disagreements, contrary to the observations with FLEX-Topo$_{WB}$, were during Green-up/ mid-Green-up and
Maturity/Peak phenophases in the rainy season with R^2 range of 0.32 – 0.77; 0.06 – 0.58 respectively. In terms of

455   Bias, with an exception of MOD16 all EBM's generally underestimated evaporation during Maturity and Peak
phenophases.
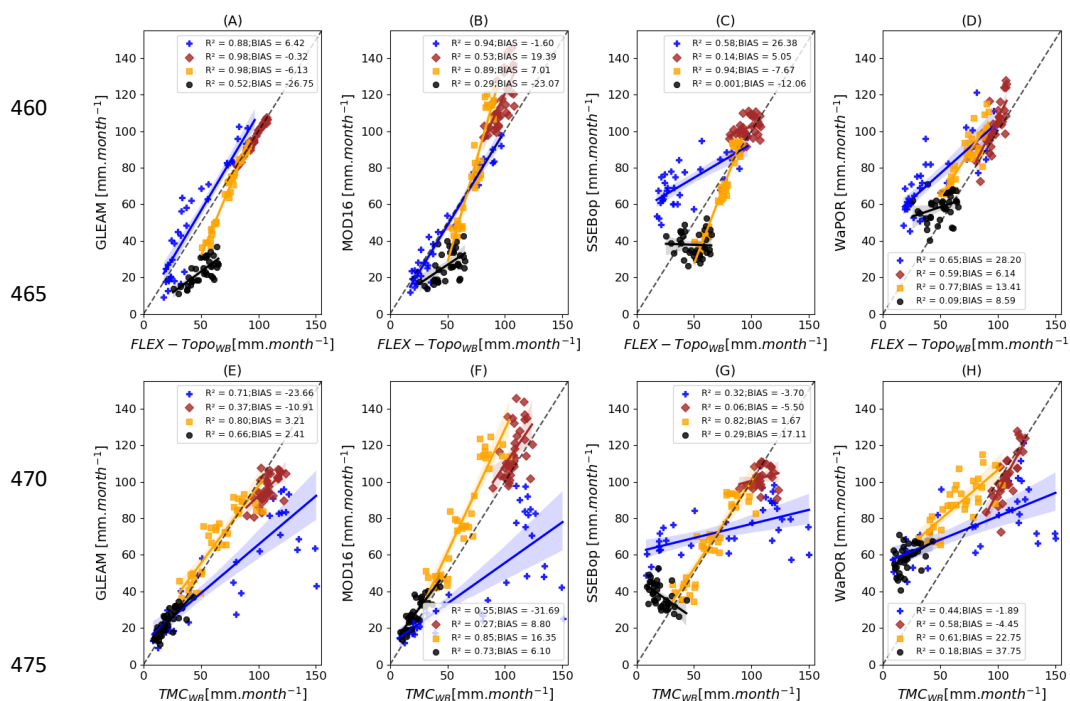
Figure 6 A. Basin scale comparison of mean monthly (2009-2020) EBM with WBM. (A-D) EBM comparison
with FLEX-Topo$_{WB}$ and (E-H) comparison with TMC$_{WB}$. Colour code: BLUE= Green-up/Mid-Green-up; BROWN
= Maturity/Peak; ORANGE = Senescence/Green-down/Mid-green-down and BLACK = Dormant phenophase.

480

     With reference to Bias, MOD16 underestimated evaporation during Green-up and Mid-Green-up
phenophases but overestimated during the rest of the phenophases with Bias range 6.10 – 31.69 mm.month[-1].
GLEAM, SSEBop and WaPOR showed mixed performance underestimating during Green-up/ mid-Green-up and
Maturity/Peak phenophases and overestimating evaporation during senescence, Mid-green down and dormant

485   phenophases with Bias range of 1.89 – 37.75 mm.month^{-1} (Figure 6). With reference to both FLEX-Topo$_{WB}$ and TMC$_{WB}$ model performance varied depending on season, i.e., rainy or dry season, and phenophase.

3.3   Spatial-temporal evaporation distribution during phenophases and model performance

    Figure 7A shows spatial-temporal distribution of NDVI and evaporation while Figure 7B shows violin
490   plots of evaporation across phenophases in the Luangwa Basin. NDVI was used as indicator of spatial-temporal transitions in vegetation greenness, canopy cover and vegetation water content across phenophases. Spatial and temporal distribution of evaporation varied among models across phenophases (Figure 7A and B). During the maturity/peak period, the MOD16 and TMC showed spatial patterns different from the NDVI and other evaporation models. In terms of distribution of evaporation values, except for MOD16, all models had similar
495   pattern and ranged between 250 mm.3-months^{-1} and 350 mm.3-months^{-1} (Figure 7A). FLEX-Topo$_{WB,}$ GLEAM and TMC$_{WB}$ showed very minimal variation in evaporation estimates. MOD16, SSEBop and WaPOR exhibited outliers at both end of the distribution. During the senescence/green-down period, spatial distribution of evaporation was similar among all models and followed NDVI pattern. During dormant phenophase, except for the SSEBop and WaPOR, the rest of the models exhibited similar spatial distribution of evaporation and appeared in tandem with
500   NDVI.

    During the maturity/peak phenophases (Figure 7 A), except for the MOD16 and TMC, distribution of evaporation estimates was relatively similar among all the models as indicated by the means, standard deviations and variation coefficient (Table A4 in the appendices). The maturity/peak phenophases occurs during the wettest period of the year i.e., between January and March (Figure 1). In the maturity/peak phenophases, MOD16 exhibited
505   the highest bias of about 19 mm.month^{-1} and 11 mm/month with reference to the FLEX-Topo$_{WB}$ and TMC$_{WB}$ respectively (Figure 7 A and Table 3). The rest of the EBM showed lower biases. With reference to the FLEX-Topo$_{WB}$ all EBM showed strong correlation with coefficients (R^2) of above 0.85 (Table 3). However, the TMC$_{WB}$ showed lower correlation coefficients (R^2) with EBMs ranging between 0.45 – 0.85 with least (0.45) correlation observed with MOD16 (Table 3). The maturity/peak phenophases exhibited lower biases among models (Table
510   3). The Senescence/Mid-Green down phenophases occurs during the transition from the rain to the dry season. During this period, evaporation distribution exhibited relatively similar means, standard deviations and variation coefficients among models. Across the basin all models estimated evaporation in the range 200 – 300 mm.3-months^{-1} during this period (Figure 7 and Table A4 in the appendices). In terms of magnitude of evaporation, compared to the maturity/peak phenophases the senescence/mid-green-down/greendown phenophases exhibited
515   lower estimates, both maximum and minimum estimates. With reference to FLEX-Topo$_{WB}$ and TMC$_{WB}$ high correlation coefficients of between 0.75 and 0.99, RMSE of between 1.2 and 8.8 mm.month^{-1}, and biases of between -7.7 and 22.7 mm.month^{-1} were noted (Figure 7A, Table 3 and Table A5 in the appendices). Compared to the other phenophases, the dormancy phenophase, normally experienced between July and September in the dry season, showed the most variations, in terms of evaporation spatial distribution and magnitude (Figure 7A and B).
520   In addition, this is the period the basin spatially experiences lowest NDVI values (Figure 7A). During dormancy phenophase, all EBM and WBM showed the lowest evaporation, exhibited distinct individual patterns and, with reference to the FLEX-Topo$_{WB}$, showed the largest range of correlation (R^2) (0.54 – 0.97) (Figure 7A, Table 3 and Table A6 in the appendices). The green-up and Mid-green up phenophases, normally occur between October and December. The start of greening up is before the start of the rains in October. In all model estimates, evaporation

525 magnitude begins to increase at the start of the green-up phenophase. However, there seem to be significant observable differences in the evaporation pattern, both in terms of distribution and magnitude. With reference to the TMC_{WB} all EBM exhibited lower maximum values though the means for WaPOR and SSEBop were relatively of similar magnitude. All EBM showed strong correlation with the TMC_{WB}, correlation coefficient range of 0.75 to 0.94, but seem to underestimate evaporation with a bias range of 1.9 to 31.7 mm.month^{-1} (Figure 7A, Table 3

530 and Table A4 in the appendices).

Generally, reference to the FLEX-Topo$_{WB}$ and TMC_{WB}, and depending on the phenological stage, all EBM showed a mixed performance of underestimating and overestimating evaporation. With reference to the FLEX-Topo$_{WB}$, with an exception of WaPOR, underestimation of evaporation appeared more pronounced in the transition period from the rainy to the dry season (i.e., Senescence/Mid-Green down phenophases) and during the dry season (Dormancy phenophase). With reference to the TMC_{WB}, all EBM, with an exception of MOD16 (during the

535 maturity/peak phenophases), appeared to underestimate evaporation during the green-up/mid-green up and the Maturity/peak phenophases in the rainy season (Figure 7B and Table 3). In terms of distribution of magnitude of evaporation, it appeared to vary with model spatial resolution. Models with relatively finer spatial resolution (i.e., MOD16, SSEBop and WaPOR) showed a wider spread of evaporation values than those with coarser resolution

540 (i.e., FLEX-Topo$_{WB}$, GLEAM and TMC_{WB} (Figure 7 B).

(a)   (b)
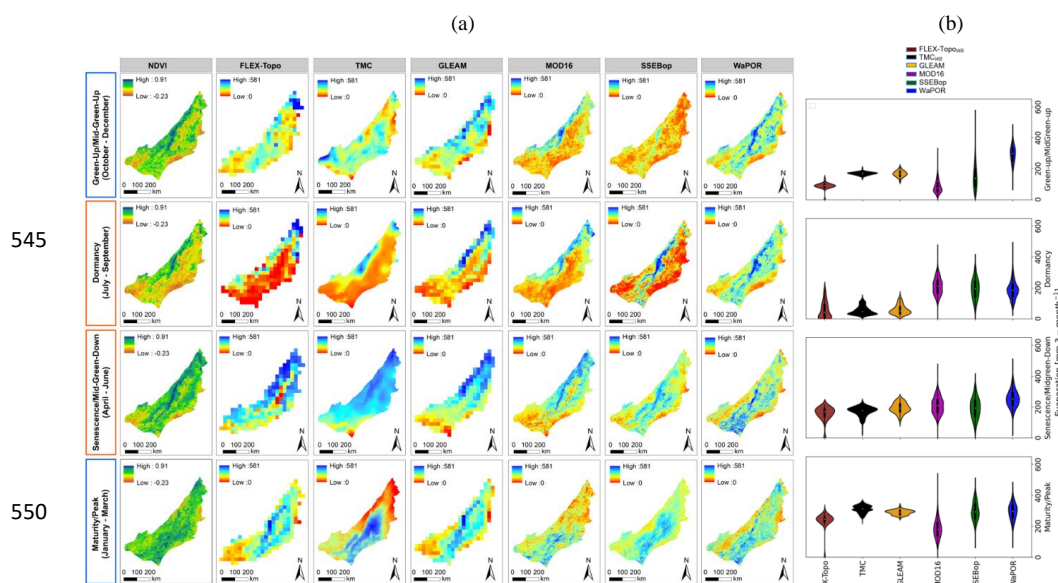
Figure 7. (A) Spatial-temporal distribution of NDVI and models evaporation (mm.3-months^{-1}) across phenophases for the year 2020 and (B) Violin plots showing variations in models' evaporation across phenophases for the year 2020 in the Luangwa Basin. Violins represent the distribution of the evaporation with indication of the median

555 (white dot), interquartile range (thick line), and 95% interval (thin line).

3.4   Land-cover based evaporation and model performance

Figure 8A and Table 3 show the 2019 Copernicus land cover map with locations of the land cover types used in this study. Figure 8B shows Google earth images of the land cover types and the number of pixels used in

560   the study for each evaporation model. Average monthly values of evaporation for the period 2009 – 2020 for each
land cover type were obtained based on pixels in a defined area (i.e., polygons) that covered the land cover of
interest.

Figure 9 shows plots of the evaporation across land cover types for each model. The evaporation pattern
based on the land cover type is very distinctive but appears to follow the basin energy and water variability cycles
565   (Figure 3). The most notable difference in land-cover based evaporation estimates by the models was observed in
the classes' dense forest and open water body. In these two environments, the WaPOR and SSEBop showed a
different upward pattern and higher evaporation values compared to the rest of the models especially in the dry
season (Figure 9 A and F). In irrigated cropland the $FLEX-Topo_{WB}$, SSEBop and WaPOR appears to respond
to irrigation activities in August during the dry season. All three models show a decline in evaporation in
570   September with $FLEX-Topo_{WB}$ continuing to decline to October while SSEBop and WaPOR showed an upward
movement after September. However, all models show a similar pattern in the rain-fed cropland in the dry season
though WaPOR exhibits relatively higher values (Figure A6 in the appendices).

Tables A6 and A7 in the appendices show the calculated statistics for each land cover. Most notable
differences statically were in the class dense forest. In dense forested environment, the WaPOR and the SSEBop
575   showed the least standard deviations (less than 14 mm.month^{-1}) and coefficients of variation (less than 13%)
(Tables A4 and A5 in the appendices). The rest of the models showed relatively higher standard deviations and
coefficients of variations of above 40 percent but not exceeding 65 percent (Table A5 in the appendices). With
regard to the mixed open forest and grassland area the overall pattern for all models was similar and exhibited high
correlations exceeding Kendall correlation coefficient of 0.8 among all models (Figure 9 B and Table A5 (ii) in
580   the appendices).

Overall, the WaPOR and SSEBop appeared to have similar patterns of evaporation across the land cover types
with strong Kendall correlation coefficients of above 0.5 across land-cover types (Tables A5 and A6 in the
appendices).

Since the dense forest class showed the most notable difference in vegetated land cover classes, we
585   statistically analysed the observed differences for each phenophase. Figure 10 shows regression plots and statistics
for each phenophase. When compared to both $FLEX-Topo_{WB}$ and TMC$_{WB}$, GLEAM showed the highest
correlation range ($R^2 = 0.26 – 0.92$) and least bias (Bias range = 0 – 11.31 mm.month^{-1}) (Figure 10 A) across
phenophases while SSEBop and WaPOR showed the least correlation ($R^2 = 0 – 0.58$) and highest bias (Bias range
= 1.79 – 56.01 mm.month^{-1}) (Figure 10 C, D, G, H). MOD16 compared well with $FLEX-Topo_{WB}$ across
590   phenophases ($R^2 = 0.41 – 0.81$; Bias = 6.23 – 26.93 mm.month^{-1}) but not so much with TMC$_{WB}$ ($R^2 = 0.38$- 0.76;
Bias range = 4.82 -38 mm.month^{-1}) (Figure 10 B and F). Generally, most model disagreements were observed
during green-up/mid-green-up and dormant phenophases.

595

Table 3. Location of field verified land cover types

Land cover type	Latitude	Longitude
Build up area	-14.42	28.45
Cropland (Rain-fed)	-14.31	31.49
Cropland (Irrigated)	-13.80	29.24
Dense forest (Miombo forest)	-12.39	31.16
Open water body	-12.96	30.75
Shrubland	-12.51	31.70
Sparse forest (Open Miombo/grassland)	-14.43	29.56

(a)

(b)
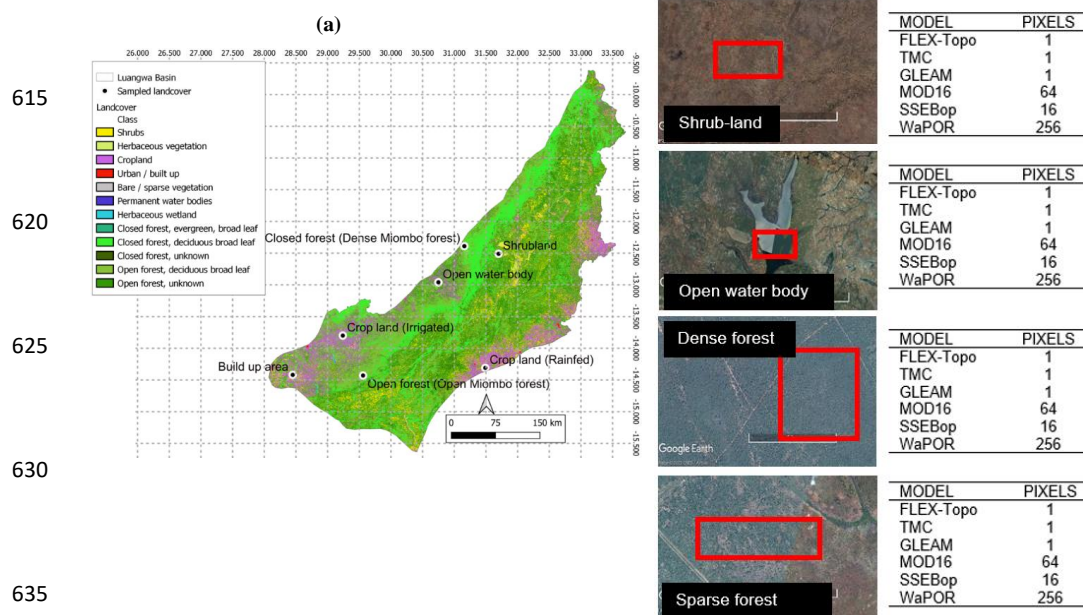
Figure 8. Verified locations (Table 3) of land cover types on the Copernicus 2019 land cover map (A) for the Luangwa Basin. © Google earth (B) was used to generate polygons based on the field verified locations for extraction of evaporation values for each model.
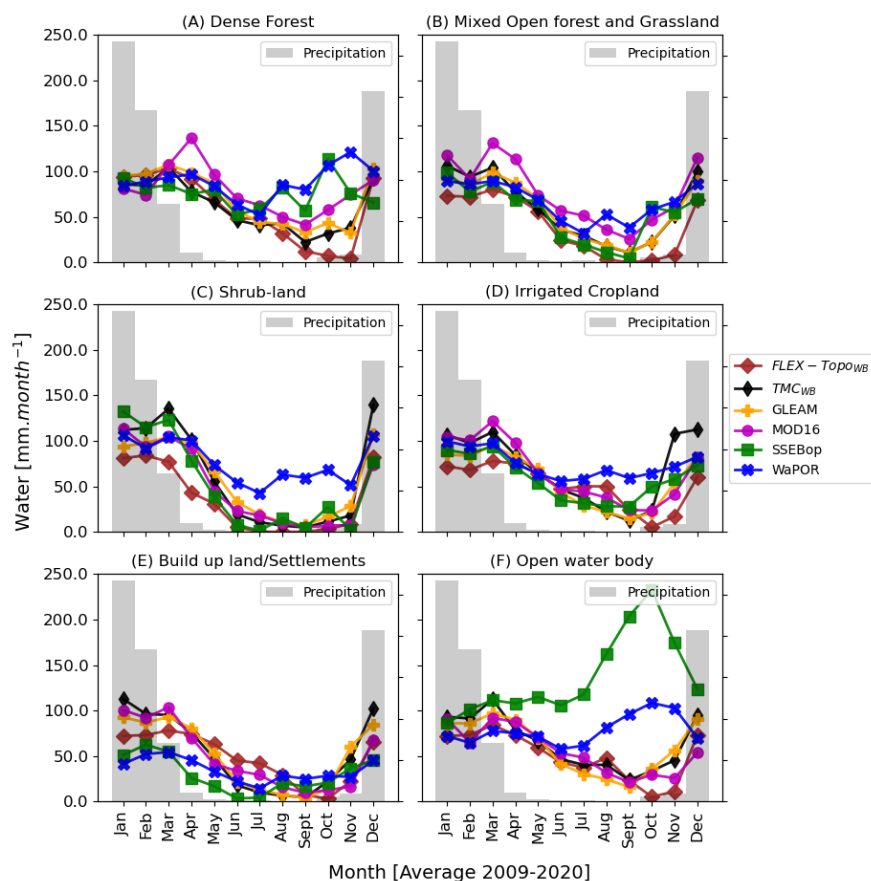
Figure 9. Land cover type dependent temporal distribution of long-term (2009-2020) mean monthly evaporation in the Luangwa Basin. Major differences, in evaporation temporal patter and magnitude between WBM and EBM as well as among EBM, seem to occur in natural vegetation i.e., Dense Miombo Woodland in the dry season (May – October).
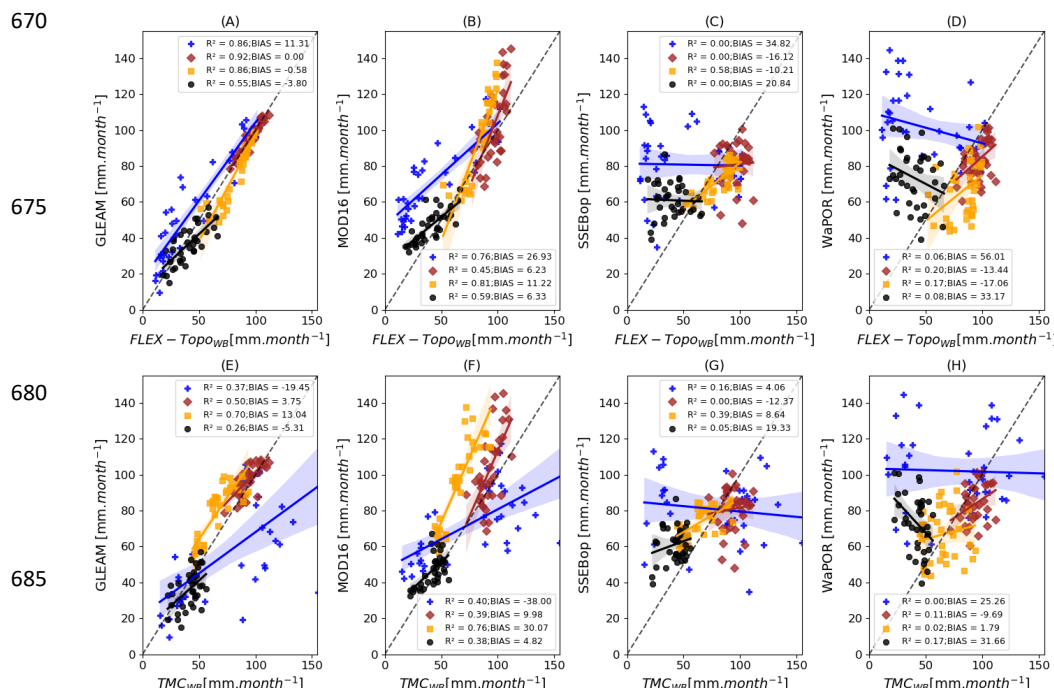
Figure 10. Relationship of EBM and WBM mean monthly (2009-2020) evaporation across seasons and phenophases in dense Miombo Woodland in the Luangwa Basin. (A-D) EBM comparison with FLEX-Topo$_{WB}$ and (E-H) comparison with TMC$_{WB.}$. Colour code: BLUE= Green-up/Mid-Green-up; BROWN = Maturity/Peak; ORANGE = Senescence/Green-down/Mid-Green-down and BLACK = Dormant phenophase.

4.0   Discussion

The objectives of this study were to evaluate evaporation models performance in the Luangwa Basin and to discuss the potential underlying factors to the observations. We discuss differences in spatial and temporal model performance and highlight potential underlying factors to the observed discrepancies.

4.1   Observations in model's performance in terms of spatial-temporal distribution of evaporation

Across seasons and phenophases, we have observed discrepancies in spatial-temporal models' performance. Precipitation and forest cover have been shown to be the main determinants of water availability at catchment level through actual evaporation rather than the potential evaporation (Zhang et al., 2001). For instance, forested areas tend to have higher evaporation than non-forested or grassland areas and this is dependent on the age and health of the trees (Teuling, 2018). In agreement with Teuling (2018) and Zhang et al. (2001) results of this study show significant land cover dependent differences in the spatial and temporal distribution of evaporation. Forested areas showed the most discrepancies in the spatial-temporal distribution pattern of evaporation in all models with the WaPOR and SSEBop exhibiting visibly distinct patterns from the other models in the dry season. Furthermore, in periods with high soil moisture and high canopy cover (i.e., maturity/peak and senescence/Green-down/mid-green down) all models performed similar. However, significant diversion in model behaviour was more pronounced during periods of limited soil moisture and low canopy cover (i.e., dormancy and green-up/mid-

green up phenophases). Documented coefficient of variation in Miombo Woodland canopy cover (i.e., as proxied

710   by the leaf area index and normalised difference vegetation index) is about 30 percent (Zimba et al., 2020; Frost, 1996). Furthermore, Miombo species leaf colour transitions and leaf fall does not occur at the same time but varies among species (i.e., Figure 11) and also depends on the amount of rainfall received in the preceding season (Frost, 1996). The field observations we made in 2021 at Mpika (Figures 2 and 11) confirmed and illustrates the differences in leaf fall/flush, leaf colour transitions and green-up at Miombo local forest level.

715
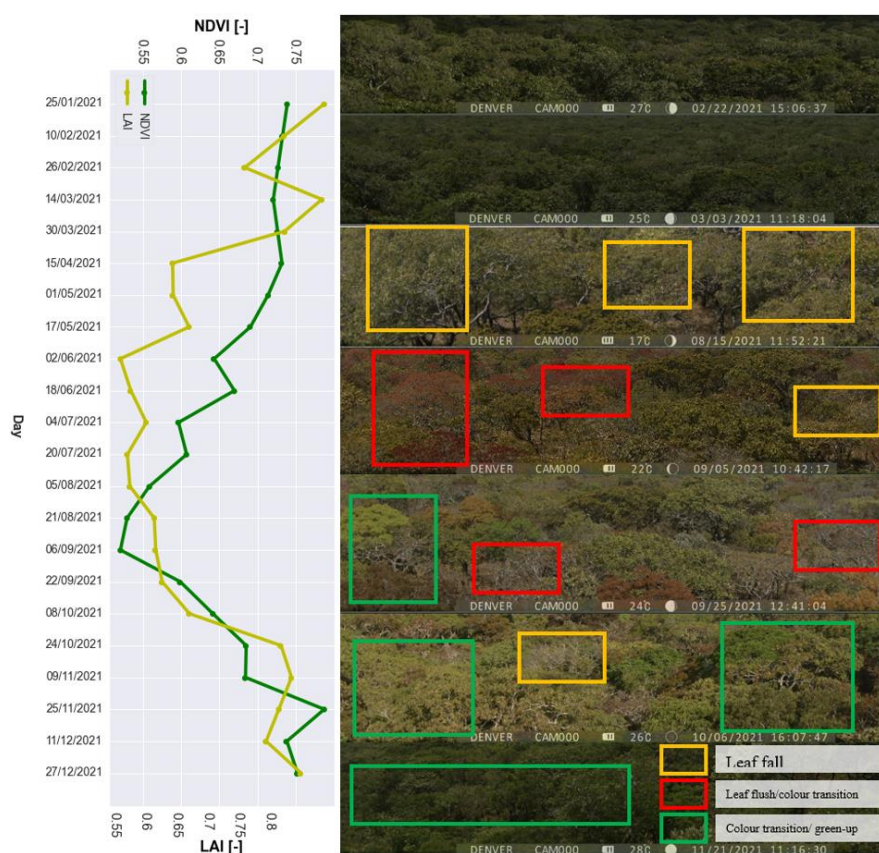
Figure 11. MODIS LAI, NDVI, and the Miombo Forest canopy display pattern for the year 2021 at Mpika station.

740

The field observations of Miombo canopy display dynamics agreed with the MODIS based LAI and NDVI pattern for the year 2021 (Figure 11). LAI and NDVI differed at the start of rise with LAI starting early in August indicating increase in leaf flush activity. Unlike the LAI, NDVI begins to rise in September indicating a delay resulting from the leaf colour transitions as exhibited in Figure 11. Implication of the leaf colour transitions,

745   variations in the time for leaf fall and the variation coefficient in canopy display is that during the dry season the Miombo Woodland, at forest/catchment level, is not completely leafless as it returns 70 percent of the canopy display (i.e., Figure 11). Tian et al. (2018) showed that while transpiration co-varies with canopy cover (i.e., leaf area index (LAI)) in the Miombo Woodland the water storage in the root zone and the body of the vegetation tends

to increase towards the end of the rain season remaining relatively constant during the dry season until the LAI
750 begins to increase again. Further, Tian et al. (2018) observed that the Miombo Plants tend to rely on the deep root
zone water during the dry period of the year. Vinya et al.(2018) showed that the stem water storage dynamics
strongly influence canopy display. Pelletier et al. (2018) and Tian et al. (2018), using different approaches, deduced
how different the Miombo Woodlands species traits are from other ecosystems; how they store water and their
interaction with the root zone storage during the dry season. Their findings, largely, could possibly explain the
755 differences we observed in the model's spatial temporal distribution of evaporation during the dry season. Forest
cover strongly influences catchment evaporation during the dry season (Zhang et al., 2001; Teuling, 2018). The
Luangwa Basin is largely covered by the Miombo Woodland (*Sustainable Management of Miombo Woodlands*,
2018; Frost, 1996). Miombo Woodland species unique attributes, i.e., stem water storage, canopy display
behaviour and interaction with root zone storage (Pelletier et al., 2018; Tian et al., 2018; Vinya et al., 2018)
760 probably accounts for the observed spatial-temporal evaporation distribution patterns by the different models in
this study.

A key underlying factor for the observed discrepancies in spatial distribution of evaporation by models is
the difference in the land cover products used. For instance, MOD16 heavily relies on a global land-cover product
(Gray et al., 2019b; Running et al., 2019) known to misclassify certain land cover types and showing low user
765 accuracy in certain regions (i.e., Leroux et al., 2014). WaPOR uses the Copernicus land cover product but adds
the distinction between irrigated and rain-fed areas (FAO, 2018). For vegetation fraction, GLEAM uses the
MODIS MOD44B product (Martens et al., 2017; Miralles et al., 2011). Dissimilarities in the land cover products
possibly reflect in differences in the models spatial distribution of evaporation.

4.2   Potential underlying factors in model performance in the Luangwa Basin

In this section, we look at model architecture and observed evaporation estimates in relation to Miombo
Woodland attributes and how this potentially explains models' performance in the Luangwa Basin.

In this study, although GLEAM consistently underestimated annual evaporation for the period 2009 –
2020, it agreed well with the $FLEX-Topo_{WB}$ and TMC_{WB} during the rain season. This suggests that the
775 underestimation observed at annual scale could be because of GLEAM behaviour during the dry season. Firstly,
GLEAM assumes a maximum root-zone soil moisture depth of 250 cm for tall vegetation i.e., the Miombo forest.
However, Miombo species in deep soils have been shown to have tap roots exceeding 5 m depth and lateral roots
covering between 15 – 25 m (Frost, 1996). Different ecosystems and land-cover types have different root zone
storage capacities to buffer drought periods (Wang-Erlandsson et al., 2016). Pelletier et al. (2018) and Tian et al.
780 (2018) showed that Miombo Woodland species potentially access ground water for various physiological activities
during the dry season. Vinya et al. (2018) showed linkage between changes in canopy display and Miombo plants
stem water storage in the dry season. The Miombo Forest largely retains its canopy cover during the dry season
(i.e., Figure 11; Zimba et al., 2020; Frost 1996). Therefore, with capacity to tap into ground water reservoirs and
stem water storage mechanisms, depending on the species, it is likely that Miombo plants continues transpiring
785 throughout the dry season. Additionally, use of the net precipitation for the running water balance to determine
root zone soil moisture implies that GLEAM evaporation is sensitive to precipitation regimes. This, in our study,
is augmented by observations in the temporal pattern of GLEAM (Figure 5) as it showed relatively, i.e., compared
to $FLEX-Topo_{WB}$, and MOD16, higher evaporation at the commencement of the rainy season during the green-

up and Mid-green-up phenophases. It also means that the quality of the rainfall product used to parameterise root-
790   zone soil moisture affects evaporation estimates. Luangwa Basin is in a sparsely gauged semi-arid environment in
Africa for which some precipitation products show large bias (Oki and Kanae, 2006). Therefore, it is likely that
GLEAM does not effectively capture the Miombo Woodland evaporation in the dry season.

     With reference E_{wb}, MOD16 showed relatively low annual bias. In addition, MOD16 showed low bias
and high correlation with the $FLEX - Topo_{WB}$ and TMC_{WB} at monthly scale for the period 2009 -2020. MOD16
795   showed mixed performance across phenophases depending on the water balance model compared with. With
$FLEX - Topo_{WB}$ the MOD16 showed underestimation in the dry season and overestimation in the rainy season.
With the TMC_{WB} the MO16 showed overestimation in the dry and underestimation in the rainy season. Like with
the other models the major discrepancy was in dry season during the dormant and green-up phenophases, most
significantly in the dense forest-land cover. During the rainy season potential sources of
800   overestimation/underestimation, with $FLEX - Topo_{WB}$ and TMC_{WB}, could be that the precipitation product used
in MOD16 either overestimates or underestimates precipitation (Oki and Kanae, 2006) in the Luangwa Basin. For
the MOD16 performance in the dry season, especially in forested areas, potential underlying factors for this
behaviour could be attributed to model phenophases characterisation and stomatal conductance thresholds. It is
possible the stomatal conductance thresholds are not correctly adjusted (i.e., low or higher than actual threshold
805   value) for the Miombo ecosystem. In addition, arid and semi-arid ecosystems, like the Miombo ecosystem in the
Luangwa Basin, are driven by moisture in the soil (Verstraeten et al., 2008; Makkeasorn et al., 2006). MOD16
does not couple canopy transpiration with soil moisture which is a potential source of underestimation especially
in view of the already discussed Miombo species interaction with root zone soil moisture during the dry season.
Discrepancy in spatial distribution of MOD16 with other models could be a result of the classification accuracy of
810   the land cover product used that may or may not correctly characterise the land cover in the Luangwa Basin.
Generally, other than the model structure, sources of error in MOD16 are likely also to be from model inputs like
the LAI, accuracy of the land cover map used, especially with regard to classification of forest cover in the Miombo
region, and meteorological data.

     At annual scale, with reference to E_{wb}, the SSEBop showed relatively low bias (Figure 4B). SSEBop
815   major spatial and temporal digression from other models was in the dry season in between the senescence and the
green-up phenophases. In contrast to other models, SSEBop showed an upward movement in evaporation starting
from August in the dormant phenophase in the dry season. The rest of the models showed a start of increase in
evaporation at the commencement of the green-up phenophase (Figure 5). In addition, with an exception of
WaPOR, the SSEBop had the second highest evaporation during the driest part of the dry season (September-
820   October). Three observations, in relation to model structure, that aid explanation for SSEBop spatial-temporal
behaviour (Figures 5B, 7, 9 and 12 A) in the Luangwa Basin include the model's land-cover based (i.e., Dense
Forest and Open water body) performance, spatial-temporal pattern of LST (Figure 12 B) and the area burnt by
fire (Figure 12 C). SSEBop depends on LST to distinguish hot and cold pixels for estimation of evaporation
(Savoca et al., 2013). Under water limited conditions, compared to non-evaporating surfaces evaporating land
825   surfaces tend to have lower LST (Rocha et al., 2020; Akinyemi, Ikanyeng, and Muro, 2019; Sun et al., 2016). The
start of rise in LST in August is preceded by a cool dry season with low net radiation (Figure 3) to aid evaporation
in both open water body and dense forested areas. The start of increase in SSEBop evaporation and LST in August
(i.e., Figure 12 D) corresponds to start in rise in both air temperature and radiation. This provides energy for

evaporation (Heck et al. 2020) from open water bodies and dense forests as demonstrated in Figure 9A & F. Dry

830   land surfaces such as dry grassland, burnt area and built up surfaces tend to have high LST which the SSEBop

classify as non-evaporating hot pixels.
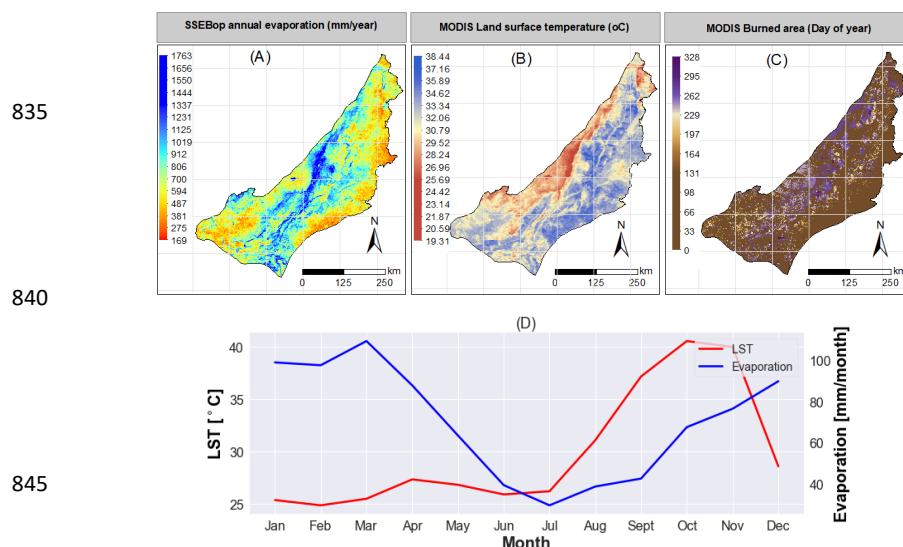
Figure 12. (A) 2020 annual SSEBop evaporation distribution, (B) annual MODIS 2020 spatial land surface

temperature distribution, (C) MODIS burned area distribution and (D) monthly temporal distribution pattern of

850   SSEBop evaporation and MODIS LST for the year 2020 in the Luangwa Basin.

This explains the spatial pattern of SSEBop evaporation during the dormant phenophases (Figure 7A)

with dense forest areas and open water bodies showing high evaporation values while dry croplands, dry grassland

and burnt areas show low or no evaporation (Figure 9). LST is also used as indicator of plant water condition and

855   soil water condition (Sun et al., 2019; Zhang et al., 2014). The SSEBop temporal behaviour in the dry season

seems to confirm that Miombo plants have a water storage mechanism and interacts with ground water systems

that facilitate the observed evaporation pattern.

With reference to E_{wb}, the WaPOR consistently overestimated annual evaporation from 2009 to 2020

with exception of 2016, 2017 and 2019 (Figure 4B). Analysis at seasonal level showed that the observed

860   overestimation at annual scale was due to the distinct model behaviour during the dry season. During the rainy

season, i.e., December to March in the Mid-green-up, maturity and peak phenophases, the WaPOR was

consistently similar with other models and relatively underestimated evaporation (compared to MOD16

and TMC_{WB}) (Figure 5). Overestimation started at the commencement of the downward movement in soil moisture

at the end of the rainy season. This behaviour remained consistent throughout the dry season across the different

865   Luangwa Basin phenophases and land-cover types. Spatial-temporal patterns (Figures 5, 7 and 9) showed WaPOR

performed distinctly differently from other models especially in dense forest areas and open water bodies. The

Luangwa Basin is largely forested (Phiri et al., 2019; Figures 8 and 13) with a diverse plant species composition

but largely Miombo Woodland species (Frost 1996; White 1984). The 2019 Copernicus land cover classification,

80 percent user accuracy and forest classification accuracy of about 75% (Buchhorn et al., 2020; Martins et al., 2020), showed that 77 % of the Luangwa Basin's 159,000 km^2 total basin area is forest (dense and open forest). The deep plant rooting depth of up to about to 25 m in some Miombo species (Frost 1996) evidences the capacity of the plants to access ground water resources in deep soils in the dry season. Retention of about 70 percent of canopy cover and the variations in time for leaf fall, leaf flush and leaf colour transitions among the Miombo species in the dry season (Zimba et al., 2020; Vinya et al., 2018, Frost, 1996) implies availability of an evaporative surface (i.e., leaves for transpiration). Forest cover is therefore a major influence on the basins hydrological feedbacks. Use of land-cover and phenology data sets and coupling of canopy transpiration with soil moisture in the root zone potentially explains the behaviour of the model in the dry season. By incorporating these aspects in its structure, the WaPOR is able to track the Miombo vegetation canopy display and phenological transitions as well as dynamic vegetation interaction with the root-zone soil moisture. The WaPOR's Miombo Woodland evaporation spatial-temporal pattern could be a correct representation of the ecosystem's moisture feedbacks. However, the question is whether the quantities estimated are correct.
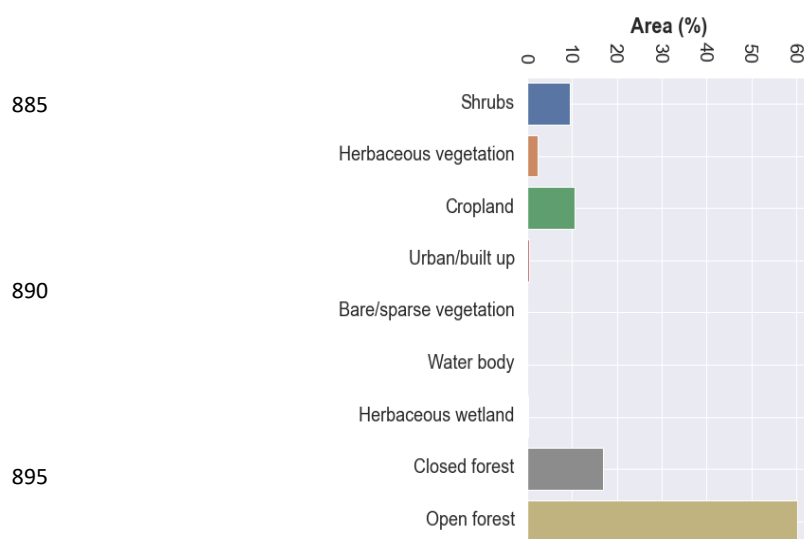
Figure 13. Copernicus 2019 land cover composition (%) in the Luangwa Basin.

Generally, there is a need to obtain land-cover specific field measurements of evaporation and associated model inputs such as precipitation, relative humidity, leaf area index, net radiation, air temperature, land surface temperature and validation of land cover maps in the Miombo ecosystem. Models performance and satellite-based model inputs can be benchmarked against the field measurements after which influence of models architecture and inputs can effectively be evaluated.

5.0 Conclusions

This study aimed at comparing performance of open-source evaporation products in the Luangwa Basin, a semi-arid largely Miombo ecosystem, across phenological phases. Selecting an evaporation product for use in Miombo Woodland river basins, especially at local catchment level, is difficult due to limited validation studies

in the region albeit with an increasingly large pool of models from which to pick. This study contributes to

910   availability of information on performance of evaporation products in the Miombo Woodland. With the data sets used in this study, major conclusions drawn are that:

(i)   Model performance varies across seasons and phenophases with significant discrepancy in evaporation model performance occurring during water limited dormant and green-up phenophases.

915   The characteristics of the phenological phases of vegetation, such as the reduction in chlorophyll, reduction in metabolic activities, leaf fall, leaf flush and leaf colour transitions coupled with vegetation interaction with the root-zone storage during these two phenophases appear to influence model performance.

(ii)   With reference to land-cover types and evaporation estimates, it appears the forest cover, in this case

920   Miombo forest, plays a significant role manifested in the differences in model performance in dense Miombo forest compared to the performance in other land cover types during the dormant and green-up phenophases. It is clear that the Miombo Woodland plant-water dynamics influences model performance.

925   (iii)   Model structure and forcing data appear to influence the spatial-temporal pattern of evaporation estimates especially during the dormant and green-up phenophases. This is clearly demonstrated by the differences in the quantities of evaporation estimates, the start of rise/increase in evaporation and the spatial pattern that appear to reflect model input behaviour especially in the dry season.

930   (iv)   Since moisture feedbacks are land surface dependent a conclusive understanding of the underlying factors for the discrepancies in model behaviour is only possible with field measurements of evaporation on various specific land cover types in the Luangwa Basin in particular and the Miombo ecosystem in general.

935   (v)   In general, our study agrees with previous studies in other African ecosystems that performance of evaporation products varies. Since evaporation products used in this study were not the same as those in the studies done in the larger Zambezi Basin, our model performance assessment is not comparable. Our study based on aggregated annual mean bias, with reference to the annual general water balance, showed the SSEBop and the WaPOR to have relatively lower aggregated bias

940   compared to other models. However, with the uncertainties in the water balance forcing data such as underestimation and overestimation of precipitation, there is a clear need for field measurements of evaporation in the Miombo ecosystem to compare with the different evaporation products. The water balance approach likely underestimated evaporation especially in the dry season, due to storage effects. Based on individual model structure and the observed performance it is highly likely that

945   SSEBop and WaPOR captures more correctly the Miombo vegetation moisture feedbacks than the other products in the dormant and green-up phenophases. However, these assumptions need verification with field measurements of evaporation, espacially in the Miombo forest.

Data availability

950   Precipitation field data at Mpika station is available on https://doi.org/10.4121/19372352.v2

Code availability

Code for FLEX-Topo model can be requested from the authors

Author contributions

Conceptualization, H.Z, H.H.G.S.; formal analysis, H.Z.; resources, H.H.G.S. and N.G; supervision, M.C.-G. and

955   B.K.; writing—original draft, H.Z.; writing—review and editing, M.C.-G., B.K., H.S., N.G, P.H and H.H.G.S.

FLEX-Topo model set up and simulations, P.H. All authors have read and agree to the published version of the

manuscript.

Competing interests

At least one of the (co-) authors is a member of the editorial board of Hydrology and Earth System Sciences.

960

Acknowledgements

This study is part of the ZAMSECUR Project, whose focus is to observe and understand the remote water resources

for enhancing water, food, and energy security in Lower Zambezi B**asin** We wish to thank the Water Resources

Management Authority (WARMA) in Zambia and the SASSCAL WeatherNet for the field data used in this study.

965

Financial support

This research was done under the ZAMSECUR Project funded by the Dutch Research Council (NOW - WOTRO)

of the Netherlands under the project number W 07.303.102.

6.0   Appendices

970

A1.0   Statistical approaches used in this study

A1.1   Analysis of trends catchment evaporation time series

The Mann-Kendall trends test (Helsel et al. 2020) (equations A1 –A6) is a commonly used non-parametric

975   test that ascertains monotonic trends in time series data. The advantage is that it does not require the data to be

normally distributed and is not responsive to abrupt changes in the time series. The null hypothesis is that there is

no trend in the series while the alternative hypothesis is that there is a trend in the series.

$$S = \sum_{i=1}^{n-1} \sum_{j=i+1}^{n} Sgn\,(x_j - x_i) \tag{A1}$$

980

Where n is the number of observations, x_j and x_i are the jth and ith observations respectively, and j > 1. Equation

3 defines the sign function Sgn between consecutive x values:

$$Sgn(x_j - x_i) = \begin{cases} +1; & x_j > x_i \\ 0; & x_j = x_i \\ -1; & x_j < x_i \end{cases} \tag{A2}$$

985   The variance is expressed by equation 4:

$$Var(S) = \frac{n(n-1)(2n+5) - \sum_{j=1}^{n} t_i\, i(i-1)(2i+5)}{18} \qquad (A3)$$

The modified variance (Var*(S)) expressed as equation 5:

990 $$Var^*(S) = Var(S).\frac{n}{n^*} \qquad (A4)$$

Where $\frac{n}{n^*}$ is the correction factor.

The test statistic Z (c) is computed by equation 6:

$$Z(c) = \begin{cases} \dfrac{S-1}{\sqrt{Var^*(S)}}, & S > 0 \\ 0, & S = 0 \\ \dfrac{S+1}{\sqrt{Var^*(S)}}, & S < 0 \end{cases} \qquad (A4)$$

995

If Z > 0, it indicates an increasing trend, and vice versa. Given a significant level of α = 0.05, the null hypothesis of a non-existent trend is accepted if -1.96 < Z(c) <1.96, for a two-tailed test.

The magnitude of each model time series trend was evaluated by a simple non-parametric procedure developed by Sen (Sen 1968; Theil 1950).

1000

$$\beta = Median\left(\frac{x_j - x_i}{j - i}\right), j > i \qquad (A6)$$

Where β is Sen's slope estimate. $\beta > 0$ indicates upward trend in a time series and $\beta < 0$ indicates downward trend during the period.

A1.2   Analysis of correlation in evaporation time series

1005   Hydrological data is known to be non-normal in distribution (Helsel et al. 2020) thus assessing correlation among hydrological variables is normally done using non-parametric test. In this study, we used the Kendall correlation statistic (Helsel et al. 2020; Kendall, 1975) to assess relationships among the various evaporation products at monthly and annual scales. Kendall's Tau is a correlation parameter that measures the strength of the relationship between variables. Kendall's Tau is performed on the ranks of the data. This implies that for each

1010   specific variable the values are put in order and numbered for instance, 1 for the lowest value, 2 for the next lowest until the nth value is numbered. As is the case with other measures of correlation, Kendall's Tau takes values between -1 and +1, in which a positive correlation indicates that the ranks of both variables increase together while a negative correlation denotes opposite directions in the ranks of the variables (rank of one variable increases, the other decreases). In essence, Kendall's Tau represents a difference between the probability that the observed data are in the same order versus the probability that the observed data are not in the same order. Kendall Tau statistic

1015   is given by equation A7.

$$\tau = \frac{n_c - n_d}{n(n-1)/2} \qquad (A7)$$

1020 where n_c denotes concordant pairs and n_d are discordant pairs. When the rank of the second variable is greater than the rank of the former variable the pair is said to be concordant. When the rank of the second variable is equal to or less than the rank of the first variable, the pair is considered discordant (Hirsch and Helsel, 2002). There were no tied values in the evaporation time series.

A1.3   Assessment of model performance

1025

To assess how close to the reference data the EBM evaporation were we used three statistical parameters; the coefficient of determination (R^2), the root mean square error (RMSE) and the bias.

The coefficient of determination (R^2) is the proportion of the difference in the modelled data that is predictable from the observed data. It is a statistical measure of how well the modelled estimates approximate the observed

1030 data. The closer to 1 the R^2 is the better the performance of the mode. R^2 is estimated using equation A8.

$$R^2 = 1 - \frac{\sum_{i=1}(X_i - Y_i)^2}{\sum_{i=1}(\bar{Y} - Y_i)^2} \qquad (A8)$$

Where, X_i is the predicted ith value, and the Y_i element is the actual ith value.

The RMSE is the square root of the summation of the square of the difference(s) between the observed

1035 and modelled values over the total number of observations (Equation 10). The RMSE quantifies the deviation of the predicted values from the observed values. The closer to zero the RMSE value is the better the model prediction(s). RMSE is estimated using equation A9.

$$RMSE = \sqrt{\frac{\sum_{i=1}^{N}(Y_i - \bar{X}_i)^2}{N}} \qquad (A9)$$

1040

Where i = variable$i$, N = number of observations, Y = actual observations time series and X is the modelled time series.

1045

1050
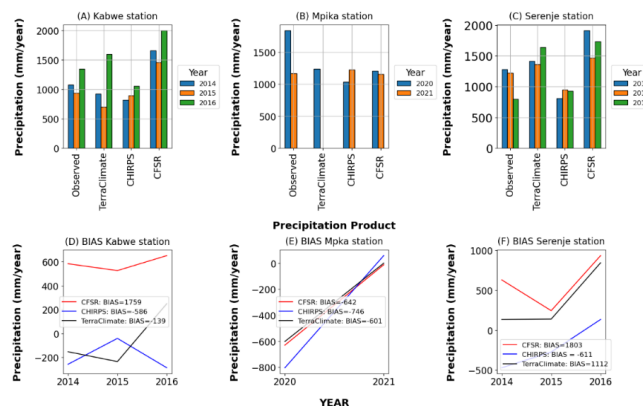
Figure A1. Comparison of observed precipitation with satellite precipitation products TerraClimate, CHIRPS and CFSR at (A) Kabwe weather station, (B) Mpika weather station and (c) Serenje weather station in the

1055 Luangwa Basin. D- F shows the aggregated annual bias for each model.
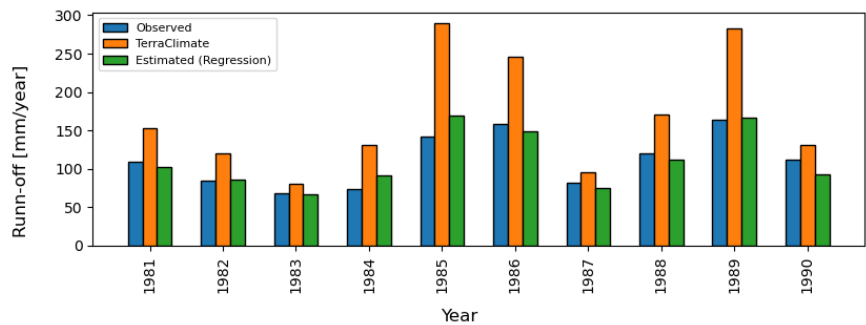
Figure A2. Comparison of TerraClimate and regression-based runoff with observed runoff for the period 1981-1990 for the Luangwa Basin.
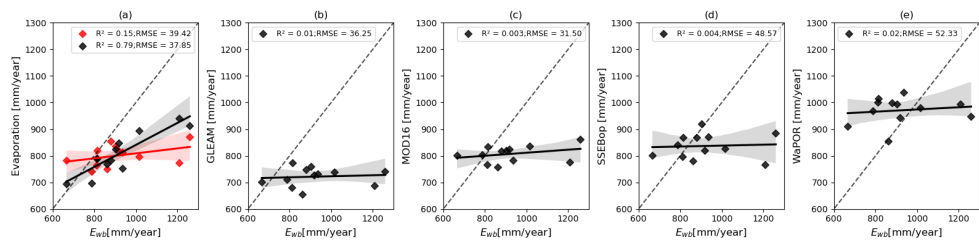
Figure A3. Comparison of E_{wb} with (a) FLEX-Topo$_{WB}$ (red) and TMC$_{WB}$ (black), (b) GLEAM, (c) MOD16, (d) SSEBop and (e) WaPOR for the period 2009 -2020.
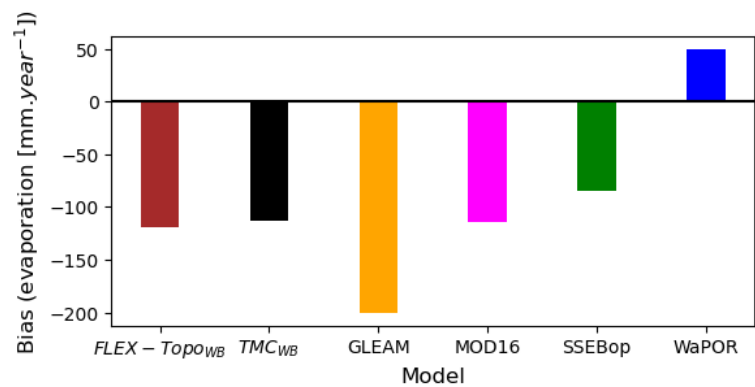
Figure A4. Comparison aggregated annual mean bias for models for the period 2009 -2020. The WaPOR showed the least overestimation aggregated bias while the SSEBop showed the least underestimation bias.

1085   **Table A1. Monthly descriptive and seasonal Mann-Kendall trends test statistics for the period 2009 -2020**

MODEL	No.	Min	Max	Mean	SD	VC	Kendall's tau	p-value	alpha	Decision
TMC	144	8.27	150.30	67.36	40.93	0.61	0.05	0.70	0.05	No trend
Flex-Topo	144	17.47	107.75	66.81	25.79	0.38	-0.13	0.11	0.05	No trend
WaPOR	144	40.51	127.90	80.90	21.09	0.26	-0.14	0.11	0.05	No trend
SSEBop	144	26.46	111.14	69.74	26.21	0.37	-0.29	0.01	0.05	downward trend
GLEAM	144	9.09	107.64	60.12	32.25	0.53	-0.10	0.23	0.05	No trend
MOD16	144	11.76	145.72	67.25	40.58	0.60	0.03	0.78	0.05	No trend

    Interpretation: *No. = number of observation, Min = minimum, Max = maximum, SD = standard deviation, VC = variation coefficient*

Table A2. Annual Pearson correlation statistics

Model	TMC	Flex-Topo	WaPOR	SSEBop	GLEAM	MOD16	Ewb
Flex-Topo	0.37						
WaPOR	0.14	0.32					
SSEBop	-0.03	**0.74**	0.46				
GLEAM	0.15	**0.77**	0.57	**0.84**			
MOD16	0.34	**0.74**	0.17	**0.64**	**0.81**		
Ewb	**0.98**	0.28	0.09	-0.14	0.03	0.20	

Values in bold are different from 0 with a significance level alpha=0.05

1090

1095

1100

1105
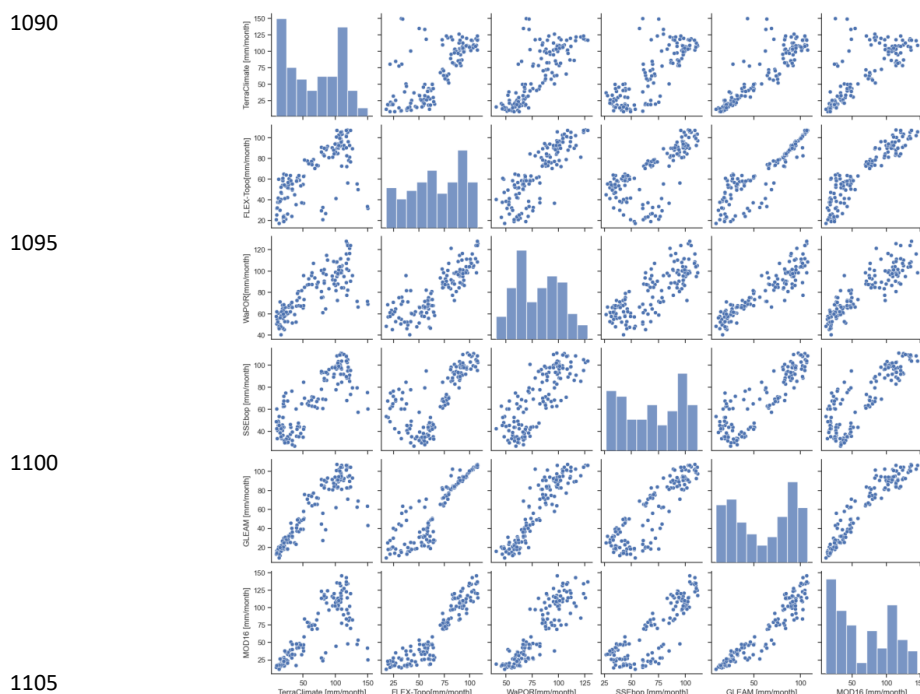
Figure A5. Kendall correlation statistics of models mean monthly evaporation for the period 2009 – 2020 in the

Luangwa Basin.

Table A3. Kendall correlation staticts for mean monthly evaporation

Model	TMC	WaPOR	SSEbop	GLEAM	FLEX-Topo	MOD16
TMC	**1**					
WaPOR	**0.62**	**1.00**				
SSEBop	**0.54**	**0.56**	**1.00**			
GLEAM	**0.73**	**0.76**	**0.64**	**1.00**		
FLEX-Topo	**0.56**	**0.66**	**0.54**	**0.77**	**1.00**	
MOD16	**0.61**	**0.70**	**0.58**	**0.80**	**0.75**	**1.00**

Values in bold are different from 0 with a significance level alpha=0.05
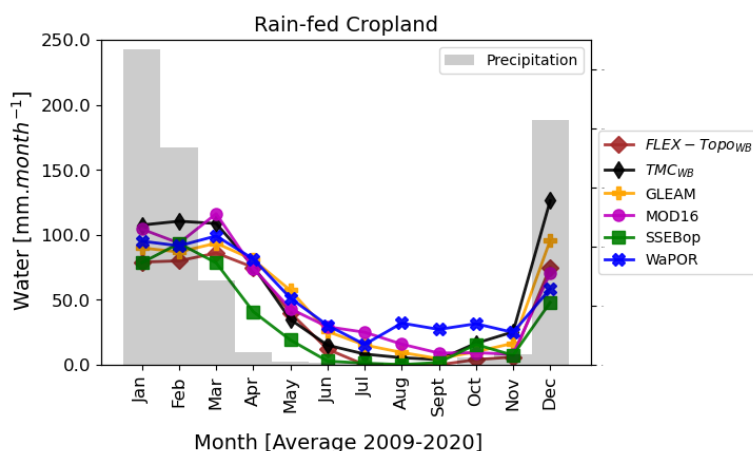
Figure A6. Mean monthly model evaporation estimates in rain-fed cropland for the period 2009 – 2020 in the Luangwa Basin.

Table A4. Calculated statistics for the phenophases, Maturity/Peak, Senescence/Mid-Green down, Dormancy, Green up/Mid-Green up

Statistic	Maturity/Peak						Senescence/Mid-Green down					
	TMC	FLEX-Topo	WaPOR	SSEBop	GLEAM	MOD16	TMC	FLEX-Topo	WaPOR	SSEBop	GLEAM	MOD16
No.	38.00	38.00	38.00	38.00	38.00	38.00	38.00	38.00	38.00	38.00	38.00	38.00
Minimum	100.91	92.30	96.89	97.70	92.12	107.54	42.34	58.52	71.50	40.99	44.03	48.06
Maximum	112.02	101.97	108.08	108.01	102.24	132.66	87.00	87.07	98.26	90.42	87.42	116.33
Sum	321.87	290.11	308.53	305.28	289.15	348.27	193.01	221.03	261.26	198.03	202.65	242.06
Mean	107.29	96.70	102.84	101.76	96.38	116.09	64.34	73.68	87.09	66.01	67.55	80.69
Standard deviation	5.74	4.89	5.63	5.50	5.24	14.36	22.34	14.35	13.91	24.72	21.92	34.23
Variation coefficient	0.04	0.04	0.04	0.04	0.04	0.10	0.28	0.16	0.13	0.31	0.27	0.35

Statistic	Dormancy						Green up/Mid-Green up					
	TMC	FLEX-Topo	WaPOR	SSEBop	GLEAM	MOD16	TMC	FLEX-Topo	WaPOR	SSEBop	GLEAM	MOD16
No. of observations	38.00	38.00	38.00	38.00	38.00	38.00	38.00	38.00	38.00	38.00	38.00	38.00
Minimum	12.86	41.24	51.58	31.71	16.07	17.54	19.65	23.83	56.44	62.30	19.28	18.45
Maximum	29.55	55.00	62.40	43.22	30.37	36.52	119.27	81.38	93.74	83.52	89.44	82.40
Sum	62.26	149.76	175.52	113.59	69.50	80.56	231.13	140.87	225.47	220.02	160.14	136.07
Mean	20.75	49.92	58.51	37.86	23.17	26.85	77.04	46.96	75.16	73.34	53.38	45.36
Standard deviation	8.38	7.55	6.01	5.79	7.15	9.50	51.51	30.39	18.65	10.64	35.13	33.16
Variation coefficient	0.33	0.12	0.08	0.12	0.25	0.29	0.55	0.53	0.20	0.12	0.54	0.60

1110

1115

1120

1125

1130

Table A5. Calculated statistics for land cover based evaporation. Table 1 A(i) are calculated statistics for the class dense forest, Table 1A(ii) for the class mixed forest and grassland, Table A(iii)for cropland, Table A(iv) for shrub-land, Table A(v) for open water body and Table A(vi) for built up area.

1135

(i) Dense forest

Statistic	TMC	FLEX-Topo	WaPOR	SSEBop	GLEAM	MOD16
No. of observations	144.00	144.00	144.00	144.00	144.00	144.00
Minimum	17.38	4.00	83.09	86.77	25.44	37.02
Maximum	112.37	103.00	126.24	125.00	108.44	149.27
Mean	61.90	58.17	107.40	103.18	66.74	87.67
Standard deviation	36.29	37.87	13.58	11.90	33.15	37.11
Variation coefficient	0.56	0.62	0.12	0.11	0.48	0.41

(ii) Mixed forest and grassland

Statistic	TMC	FLEX-Topo	WaPOR	SSEBop	GLEAM	MOD16
No. of observations	144.00	144.00	144.00	144.00	144.00	144.00
Minimum	10.62	0.00	31.86	4.09	10.50	25.65
Maximum	106.22	80.00	89.31	98.59	98.48	131.02
Mean	58.85	39.67	66.19	53.95	57.48	76.56
Standard deviation	36.17	32.96	20.88	31.13	33.08	35.87
Variation coefficient	0.59	0.80	0.30	0.55	0.55	0.45

(iii) Crop land

Statistic	TMC	FLEX-Topo	WaPOR	SSEBop	GLEAM	MOD16
No. of observations	144.00	144.00	144.00	144.00	144.00	144.00
Minimum	4.01	0.00	15.65	0.16	4.69	8.06
Maximum	126.22	86.00	99.14	93.39	95.81	116.24
Mean	53.19	38.08	53.24	32.28	48.83	49.90
Standard deviation	48.41	37.75	30.87	34.62	38.31	40.01
Variation coefficient	0.87	0.95	0.56	1.03	0.75	0.77

(iv) Shrub-Land

Statistic	TMC	FLEX-Topo	WaPOR	SSEBop	MOD16	GLEAM
No. of observations	144.00	144.00	144.00	144.00	144.00	144.00
Minimum	4.73	0.00	42.59	1.14	4.98	7.08
Maximum	139.52	84.00	106.30	132.31	113.64	107.12
Mean	60.68	34.58	76.67	51.87	49.29	56.77
Standard deviation	55.20	36.73	23.63	50.70	43.05	41.18
Variation coefficient	0.87	1.02	0.30	0.94	0.84	0.69

(v) Open water body

Statistic	TMC	FLEX-Topo	WaPOR	SSEBop	GLEAM	MOD16
No. of observations	144.00	144.00	144.00	144.00	144.00	144.00
Minimum	23.34	5.00	57.68	86.07	15.61	21.20
Maximum	112.23	84.00	108.31	232.82	96.75	91.74
Mean	63.78	50.08	78.08	136.76	60.20	55.59
Standard deviation	29.31	26.64	16.23	45.76	29.74	25.72
Variation coefficient	0.44	0.51	0.20	0.32	0.47	0.44

	(vi)	Build-up land				
Statistic	TMC	FLEX-Topo	WaPOR	SSEBop	GLEAM	MOD16
No. of observations	144.00	144.00	144.00	144.00	144.00	144.00
Minimum	4.51	3.00	14.18	3.25	3.46	9.59
Maximum	112.68	78.00	54.22	62.37	92.87	103.64
Mean	52.93	47.75	34.62	29.74	50.73	49.25
Standard deviation	41.38	27.10	12.72	19.80	36.62	35.73
Variation coefficient	0.75	0.54	0.35	0.64	0.69	0.69

1140

Table A6. Matrix of calculated Kendall correlation statistics for land cover based evaporation: (i) calculated statistics for the class dense forest, (ii) for the class mixed forest and grassland, (iii) for cropland, (iv) for shrub-land, (v) for open water body and (vi) for built up area.

1145

	(i)	Dense Forest					(ii)	Mixed Open forest/grassland					(iii)	Cropland				
Model	TMC	FLEX-Topo	WaPOR	SSEBop	GLEAM	MOD16	TMC	FLEX-Topo	WaPOR	SSEBop	GLEAM	MOD16	TMC	FLEX-Topo	WaPOR	SSEBop	GLEAM	MOD16
TMC	1.00	0.81	-0.12	0.03	0.88	0.70	1.00	0.81	0.82	0.88	0.94	0.94	1.00	0.78	0.58	0.79	0.85	0.58
FLEX-Topo		1.00	-0.32	0.14	0.81	0.56		1.00	0.69	0.75	0.84	0.84		1.00	0.75	0.81	0.81	0.75
WaPOR			1.00	0.24	-0.12	0.06			1.00	0.82	0.82	0.82			1.00	0.67	0.61	0.82
SSEBop				1.00	0.03	0.09				1.00	0.82	0.82				1.00	0.64	0.61
GLEAM					1.00	0.64					1.00	1.00					1.00	0.73
MOD16						1.00						1.00						1.00

Values in bold are different from 0 with a significance level alpha=0.05

1150

	(iv)	Shrub-Land					(v)	pen water body					(vi)	Built up area				
Model	TMC	FLEX-Topo	WaPOR	SSEBop	MOD16	GLEAM	TMC	FLEX-Topo	WaPOR	SSEBop	GLEAM	MOD16	TMC	FLEX-Topo	WaPOR	SSEBop	GLEAM	MOD16
TMC	1.00	0.85	0.64	0.61	0.70	0.94	1.00	0.76	-0.21	-0.52	0.79	0.70	1.00	0.55	0.55	0.61	0.82	0.70
FLEX-Topo		1.00	0.60	0.64	0.67	0.79		1.00	-0.29	-0.51	0.70	0.67		1.00	0.64	0.39	0.67	0.85
WaPOR			1.00	0.85	0.58	0.58			1.00	0.52	-0.12	-0.15			1.00	0.64	0.61	0.61
SSEBop				1.00	0.73	0.55				1.00	-0.36	-0.64				1.00	0.67	0.48
MOD16					1.00	0.70					1.00	0.61					1.00	0.82
GLEAM						1.00						1.00						1.00

Values in bold are different from 0 with a significance level alpha=0.05

References

Abatzoglou, John T., Solomon Z. Dobrowski, Sean A. Parks, and Katherine C. Hegewisch. 2018. "TerraClimate, a High-Resolution Global Dataset of Monthly Climate and Climatic Water Balance from 1958-2015." *Scientific Data* 5: 1–12. https://doi.org/10.1038/sdata.2017.191.

Abrams, Michael, and Robert Crippen. 2019. "ASTER Global DEM (Digital Elevation Mode) - Quick Guide for V3." *California Institute of Technology* 3 (July): 10.

Akinyemi, Felicia O., Mphoentle Ikanyeng, and Javier Muro. 2019. "Land Cover Change Effects on Land Surface Temperature Trends in an African Urbanizing Dryland Region." *City and Environment Interactions* 4 (2019): 100029. https://doi.org/10.1016/j.cacint.2020.100029.

Bastiaanssen W.G.M., M. Meneti, R.A. Feddes, and a a M Holtslag. 1998. "A Remote Sensing Surface Energy Balance Algorithm for Land (SEBAL){{}{{}{}{}}{{}{}{$}{}}{{}{}{}}{}}\backslashbackslashbackslashbackslashbackslash{\{}\backslash{\{}{\}}\backslashbackslash{\{}\backslash{\{}{\}}{\{}\backslash{\}}{\}}\backslashbackslashbackslash{\{ ." *J. Hydrol.* 212–213 (JANUARY): 198–212.

Beilfuss, Richard. 2012. "A Risky Climate for Southern African Hydro ASSESSING HYDROLOGICAL RISKS AND A Risky Climate for Southern African Hydro," no. September. https://doi.org/10.13140/RG.2.2.30193.48486.

Blatchford, Megan L., Chris M. Mannaerts, Sammy M. Njuki, Hamideh Nouri, Yijian Zeng, Henk Pelgrum, Steven Wonink, and Poolad Karimi. 2020. "Evaluation of WaPOR V2 Evapotranspiration Products across Africa." *Hydrological Processes* 34 (15): 3200–3221. https://doi.org/10.1002/hyp.13791.

Bowen, I. S. 1926. "The Ratio of Heat Losses by Conduction and by Evaporation from Any Water Surface." *Physical Review* 27 (6): 779–87. https://doi.org/10.1103/PhysRev.27.779.

Buchhorn, M.; Smets, B.; Bertels, L.; De Roo, B.; Lesiv, M.; Tsendbazar, N.E., Linlin, L., Tarko, A. 2020. "Copernicus Global Land Service: Land Cover 100m: Version 3 Globe 2015-2019: Product User Manual." Zenodo, Geneve, Switzerland. https://doi.org/10.5281/zenodo.3938963.

Chidumayo, E. N. 1987. "Species Structure in Zambian Miombo Woodland." *Journal of Tropical Ecology* 3 (2): 109–18. https://doi.org/10.1017/S0266467400001838.

Chidumayo, Emmanuel N., and Davison J. Gumbo. 2010. *The Dry Forests and Woodlands of Africa: Managing for Products and Services. The Dry Forests and Woodlands of Africa: Managing for Products and Services*. https://doi.org/10.4324/9781849776547.

Coenders-Gerrits, Miriam, Bart Schilperoort, and César Jiménez-Rodríguez. 2020. "Evaporative Processes on Vegetation: An Inside Look." In *Precipitation Partitioning by Vegetation: A Global Synthesis*, edited by John T Van Stan II, Ethan Gutmann, and Jan Friesen, 35–48. Cham: Springer International Publishing. https://doi.org/10.1007/978-3-030-29702-2_3.

Didan, K. 2015. "MOD13Q1 MODIS/Terra Vegetation Indices 16-Day L3 Global 250m SIN Grid V006 [Data

Set].” *NASA EOSDIS Land Processes DAAC*.

Dile, Yihun T., Essayas K. Ayana, Abeyou W. Worqlul, Hua Xie, R. Srinivasan, Nicole Lefore, Liangzhi You,
and Neville Clarke. 2020. “Evaluating Satellite-Based Evapotranspiration Estimates for Hydrological
1190   Applications in Data-Scarce Regions: A Case in Ethiopia.” *Science of the Total Environment* 743: 140702.
https://doi.org/10.1016/j.scitotenv.2020.140702.

Dyck, S. 1972. “Report on Evaporation.” *Hydrological Sciences Bulletin* 17 (1): 51–59.
https://doi.org/10.1080/02626667209493802.

Ent, Rudi J. Van Der, Hubert H.G. Savenije, Bettina Schaefli, and Susan C. Steele-Dunne. 2010. “Origin and
1195   Fate of Atmospheric Moisture over Continents.” *Water Resources Research* 46 (9): 1–12.
https://doi.org/10.1029/2010WR009127.

FAO. 2018. *WaPOR Database Methodology: Level 1 Data. Remote Sensing for Water Productivity Technical
Report: Methodology Series.* http://www.fao.org/fileadmin/user_upload/faoweb/RS-
WP/pdf_files/Web_WaPOR-beta_Methodology_document_Level1.pdf.

1200   Fisher, Joshua B, Kevin P Tu, and Dennis D Baldocchi. 2008. “Global Estimates of the Land – Atmosphere
Water Flux Based on Monthly AVHRR and ISLSCP-II Data , Validated at 16 FLUXNET Sites” 112: 901–
19. https://doi.org/10.1016/j.rse.2007.06.025.

Foken, Thomas, Marc Aubinet, and Ray Leuning. 2012. “Eddy Covariance.” *Eddy Covariance*.
https://doi.org/10.1007/978-94-007-2351-1.

1205   Frost, P. 1996. “The Ecology of Miombo Woodlands.” *The Miombo in Transition: Woodlands and Welfare in
Africa*, no. January 1996: 266. http://books.google.com/books?hl=nl&lr=&id=rpildJJVdU4C&pgis=1.

Funk, Chris, Pete Peterson, Martin Landsfeld, Diego Pedreros, James Verdin, Shraddhanand Shukla, Gregory
Husak, et al. 2015. “The Climate Hazards Infrared Precipitation with Stations - A New Environmental
Record for Monitoring Extremes.” *Scientific Data* 2: 1–21. https://doi.org/10.1038/sdata.2015.66.

1210   Gerrits, A. M.J., H. H.G. Savenije, L. Hoffmann, and L. Pflster. 2007. “New Technique to Measure Forest Floor
Interception - An Application in a Beech Forest in Luxembourg.” *Hydrology and Earth System Sciences*
11 (2): 695–701. https://doi.org/10.5194/hess-11-695-2007.

Giglio, L., Justice, C., Boschetti, L., Roy, D. 2015. “MCD64A1 MODIS/Terra+Aqua Burned Area Monthly L3
Global 500m SIN Grid V006 [Data Set].” *NASA EOSDIS Land Processes DAAC*.
1215   https://doi.org/10.5067/MODIS/MCD64A1.006.

Giliba, Richard A, Emmanuel K Boon, Canisius J Kayombo, Emmanuel B Musamba, Almas M Kashindye, and
Philipina F Shayo. 2011. “\376\377\000J\000B\000D\000-\0000\0002\000-\0001\000-
\0000\0000\0001\000-\0001\0001\000-\0000\0001\0006\000-\000G\000i\000l\000i\000b\000a\000-
\000R\000-\000A\000-\000T\000t\000.\000p\000m\000d” 2 (1): 1–7. http://www.krepublishers.com/02-
1220   Journals/JBD/JBD-02-0-000-11-Web/JBD-02-1-000-11-Abst-PDF/JBD-02-1-001-11-016-Giliba-R-
A/JBD-02-1-001-11-016-Giliba-R-A-Tt.pdf.

Gonçalves, Francisco M.P., Rasmus Revermann, Amândio L. Gomes, Marcos P.M. Aidar, Manfred Finckh, and Norbert Juergens. 2017. "Tree Species Diversity and Composition of Miombo Woodlands in South-Central Angola: A Chronosequence of Forest Recovery after Shifting Cultivation." *International Journal of Forestry Research* 2017. https://doi.org/10.1155/2017/6202093.

Granger, R. J., and N. Hedstrom. 2010. "Modelling Hourly Rates of Lake Evaporation." *Hydrology and Earth System Sciences Discussions* 7 (3): 2727–46. https://doi.org/10.5194/hessd-7-2727-2010.

Gray, J., D. Sulla-Menashe, and M. A. Friedl. 2019. "MODIS Land Cover Dynamics (MCD12Q2) Product." *User Guide Collection 6* 6: 8. https://modis-land.gsfc.nasa.gov/pdf/MCD12Q2_Collection6_UserGuide.pdf.

Gumbo, D.J., Marc Dumas-Johansen, Giulia Muir, Fritjof Boerstler, and Z. Xia. 2018. *Sustainable Management of Miombo Woodlands-Food Security, Nutrition and Wood Energy. Food Security, Nutrition and Wood Energy.* www.fao.org/publications.

Heck, K., E. Coltman, J. Schneider, and R. Helmig. 2020. "Influence of Radiation on Evaporation Rates: A Numerical Analysis." *Water Resources Research.* https://doi.org/10.1029/2020WR027332.

Helsel, D. R., R. M. Hirsch, K.R. Ryberg, S.A. Archfield, and E.J. Gilroy. 2020. "Statistical Methods in Water Resources Techniques and Methods 4 – A3." *USGS Techniques and Methods.*

Hulsman, Petra, Markus Hrachowitz, and Hubert H.G. Savenije. 2021. "Improving the Representation of Long-Term Storage Variations With Conceptual Hydrological Models in Data-Scarce Regions." *Water Resources Research* 57 (4). https://doi.org/10.1029/2020WR028837.

Hulsman, Petra, Hessel C. Winsemius, Claire I. Michailovsky, Hubert H.G. Savenije, and Markus Hrachowitz. 2020. "Using Altimetry Observations Combined with GRACE to Select Parameter Sets of a Hydrological Model in a Data-Scarce Region." *Hydrology and Earth System Sciences* 24 (6): 3331–59. https://doi.org/10.5194/hess-24-3331-2020.

Jiménez-Rodríguez, César Dionisio, Miriam Coenders-Gerrits, Bart Schilperoort, Adriana Del Pilar González-Angarita, and Hubert Savenije. 2021. "Vapor Plumes in a Tropical Wet Forest: Spotting the Invisible Evaporation." *Hydrology and Earth System Sciences* 25 (2): 619–35. https://doi.org/10.5194/hess-25-619-2021.

Jiménez, C., C. Prigent, B. Mueller, S. I. Seneviratne, M. F. McCabe, E. F. Wood, W. B. Rossow, et al. 2011. "Global Intercomparison of 12 Land Surface Heat Flux Estimates." *Journal of Geophysical Research Atmospheres* 116 (2): 1–27. https://doi.org/10.1029/2010JD014545.

Kalma, Jetse D., Tim R. McVicar, and Matthew F. McCabe. 2008. "Estimating Land Surface Evaporation: A Review of Methods Using Remotely Sensed Surface Temperature Data." *Surveys in Geophysics* 29 (4–5): 421–69. https://doi.org/10.1007/s10712-008-9037-z.

Lakhiar, Imran Ali, Ali Buttar, Ali Lakhiar, Asad Ali, Asad Ali, Muhammad Aleem, and Muhammad Asim. 2018. "Estimation of Evapotranspiration Using Bowen Ratio Method Estimation of Ratio Estimation of

Using Method Estimation of Evapotranspiration Evapotranspiration Using Bowen Bowen." *IFAC-PapersOnLine* 51 (17): 807–10. https://doi.org/10.1016/j.ifacol.2018.08.096.

Leroux, Louise, Audrey Jolivot, Agnès Bégué, Danny Lo Seen, and Bernardin Zoungrana. 2014. "How Reliable Is the MODIS Land Cover Product for Crop Mapping Sub-Saharan Agricultural Landscapes?" *Remote Sensing* 6 (9): 8541–64. https://doi.org/10.3390/rs6098541.

Liu, Wenbin, Lei Wang, Jing Zhou, Yanzhong Li, Fubao Sun, Guobin Fu, Xiuping Li, and Yan Fang Sang. 2016. "A Worldwide Evaluation of Basin-Scale Evapotranspiration Estimates against the Water Balance Method." *Journal of Hydrology* 538: 82–95. https://doi.org/10.1016/j.jhydrol.2016.04.006.

Makkeasorn, Ammarin, Ni Bin Chang, Mark Beaman, Chris Wyatt, and Charles Slater. 2006. "Soil Moisture Estimation in a Semiarid Watershed Using RADARSAT-1 Satellite Imagery and Genetic Programming." *Water Resources Research* 42 (9): 1–15. https://doi.org/10.1029/2005WR004033.

Makkink, G.F. 1957. "Testing the Penman Formula by Means of Lysimeters." *Journal of the Institution of Water Engineers* 11 (3): 277–88.

Mapaure, I. 2001. "Small-Scale Variations in Species Composition of Miombo Woodland in Sengwa, Zimbabwe: The Influence of Edaphic Factors, Fire and Elephant Herbivory." *Systematics and Geography of Plants* 71 (2): 935–47.

Martens, Brecht, Diego G. Miralles, Hans Lievens, Robin Van Der Schalie, Richard A.M. De Jeu, Diego Fernández-Prieto, Hylke E. Beck, Wouter A. Dorigo, and Niko E.C. Verhoest. 2017. "GLEAM v3: Satellite-Based Land Evaporation and Root-Zone Soil Moisture." *Geoscientific Model Development* 10 (5): 1903–25. https://doi.org/10.5194/gmd-10-1903-2017.

Martins, João Paulo, Isabel Trigo, and Sandra Coelho e Freitas. 2020. "Copernicus Global Land Operations "Vegetation and Energy" 'CGLOPS-1.'" *Copernicus Global Land Operations*, 1–93. https://doi.org/10.5281/zenodo.3938963.PU.

McCabe, Matthew F. 2019. "Advances in the Remote Sensing of Terrestrial Evaporation," 1–8. https://doi.org/10.3390/rs11091138.

McCabe, Matthew F., and Eric F. Wood. 2006. "Scale Influences on the Remote Estimation of Evapotranspiration Using Multiple Satellite Sensors." *Remote Sensing of Environment* 105 (4): 271–85. https://doi.org/10.1016/j.rse.2006.07.006.

Miralles, D. G., W. Brutsaert, A. J. Dolman, and J. H. Gash. 2020. "On the Use of the Term 'Evapotranspiration.'" *Water Resources Research* 56 (11). https://doi.org/10.1029/2020WR028055.

Miralles, D. G., R. A.M. De Jeu, J. H. Gash, T. R.H. Holmes, and A. J. Dolman. 2011. "Magnitude and Variability of Land Evaporation and Its Components at the Global Scale." *Hydrology and Earth System Sciences* 15 (3): 967–81. https://doi.org/10.5194/hess-15-967-2011.

Miralles, D. G., C. Jiménez, M. Jung, D. Michel, A. Ershadi, M. F. Mccabe, M. Hirschi, et al. 2016. "The WACMOS-ET Project - Part 2: Evaluation of Global Terrestrial Evaporation Data Sets." *Hydrology and*

Earth System Sciences 20 (2): 823–42. https://doi.org/10.5194/hess-20-823-2016.

Moors, E. 2012. "Water Use of Forests in the Netherlands." *De Vrije Universiteit Amsterdam*, 291.

Mu, Qiaozhen, Faith Ann Heinsch, Maosheng Zhao, and Steven W. Running. 2007. "Development of a Global
1295   Evapotranspiration Algorithm Based on MODIS and Global Meteorology Data." *Remote Sensing of Environment* 111 (4): 519–36. https://doi.org/10.1016/j.rse.2007.04.015.

Mu, Qiaozhen, Maosheng Zhao, and Steven W. Running. 2011. "Improvements to a MODIS Global Terrestrial Evapotranspiration Algorithm." *Remote Sensing of Environment* 115 (8): 1781–1800. https://doi.org/10.1016/j.rse.2011.05.019.

1300   Oki, Taikan, and Shinjiro Kanae. 2006. "Global Hydrological Cycles and World Water Resources." *Science* 313 (5790): 1068–72. https://doi.org/10.1126/science.1128845.

Pagán, Brianna R., Wouter H. Maes, Pierre Gentine, Brecht Martens, and Diego G. Miralles. 2019. "Exploring the Potential of Satellite Solar-Induced Fluorescence to Constrain Global Transpiration Estimates." *Remote Sensing* 11 (4). https://doi.org/10.3390/rs11040413.

1305   Pelletier, Johanne, Alain Paquette, Keddy Mbindo, Noah Zimba, Abel Siampale, Bwalya Chendauka, Freddie Siangulube, and Jonathan Wesley Roberts. 2018. "Carbon Sink despite Large Deforestation in African Tropical Dry Forests (Miombo Woodlands)." *Environmental Research Letters* 13 (9). https://doi.org/10.1088/1748-9326/aadc9a.

Phiri, Darius, Justin Morgenroth, and Cong Xu. 2019. "Long-Term Land Cover Change in Zambia: An
1310   Assessment of Driving Factors." *Science of the Total Environment* 697: 134206. https://doi.org/10.1016/j.scitotenv.2019.134206.

Rocha, Nájila Souza da, Pâmela S. Käfer, Drazen Skokovic, Gustavo Veeck, Lucas Ribeiro Diaz, Eduardo André Kaiser, Cibelle Machado Carvalho, et al. 2020. "The Influence of Land Surface Temperature in Evapotranspiration Estimated by the S-SEBI Model." *Atmosphere* 11 (10): 1059.
1315   https://doi.org/10.3390/atmos11101059.

Running, Steven W, Qiaozhen Mu, Maosheng Zhao, Alvaro Moreno. 2019. "User ' s Guide MODIS Global Terrestrial Evapotranspiration (ET) Product NASA Earth Observing System MODIS Land Algorithm (For Collection 6)."

Saha, Suranjana, Shrinivas Moorthi, Xingren Wu, Jiande Wang, Sudhir Nadiga, Patrick Tripp, David Behringer,
1320   et al. 2014. "The NCEP Climate Forecast System Version 2." *Journal of Climate* 27 (6): 2185–2208. https://doi.org/10.1175/JCLI-D-12-00823.1.

Savenije, H. H.G. 2010. "HESS Opinions 'Topography Driven Conceptual Modelling (FLEX-Topo).'" *Hydrology and Earth System Sciences* 14 (12): 2681–92. https://doi.org/10.5194/hess-14-2681-2010.

Savenije, Hubert H.G. 2004. "The Importance of Interception and Why We Should Delete the Term
1325   Evapotranspiration from Our Vocabulary." *Hydrological Processes* 18 (8): 1507–11. https://doi.org/10.1002/hyp.5563.

Savoca, M. E., G. B. Senay, M. A. Maupin, J. F. Kenny, and C. A. Perry. 2013. "Actual Evapotranspiration
Modeling Using the Operational Simplified Surface Energy Balance (SSEBop) Approach." *U.S*
Geologica Survey Scientific Investigations Report 2013–5126, no. January: 16 p.
1330   http://pubs.usgs.gov/sir/2013/5126.

Sen, Pranab Kumar. 1968. "Estimates of the Regression Coefficient Based on Kendall's Tau." *Journal of the*
American Statistical Association 63 (324): 1379–89. https://doi.org/10.1080/01621459.1968.10480934.

Smets Bert De Roo, Bruno. 2020. "CGLS-LC100 Version 3 ATBD," 1–152.
https://doi.org/10.5281/zenodo.3938968.PU.

1335   Spittlehouse, D. L., and T. A. Black. 1980. "Evaluation of the Bowen Ratio/Energy Balance Method for
Determining Forest Evapotranspiration." *Atmosphere - Ocean* 18 (2): 98–116.
https://doi.org/10.1080/07055900.1980.9649081.

Sun, Hao, Baichi Zhou, and Hongxing Liu. 2019. "Spatial Evaluation of Soil Moisture (SM), Land Surface
Temperature (LST), and LST-Derived SM Indexes Dynamics during SMAPVEX12." *Sensors*
1340   *(Switzerland)* 19 (5). https://doi.org/10.3390/s19051247.

Sun, Zhigang, Qinxue Wang, Ochirbat Batkhishig, and Zhu Ouyang. 2016. "Relationship between
Evapotranspiration and Land Surface Temperature under Energy- and Water-Limited Conditions in Dry
and Cold Climates." *Advances in Meteorology* 2016. https://doi.org/10.1155/2016/1835487.

Suranjana Saha, ShrinivaS Moorthi, hua-Lu Pan, Xingren Wu, jiande Wang, Sudhir nadiga, Patrick triPP, robert
1345   kiStLer, john WooLLen, david behringer, haiXia Liu, diane StokeS, boyin huang robert gruMbine, george
gayno, jun Wang, yu-tai hou, hui-ya chuang, hann-Ming h. juang, joe SeLa, Mark iredeLL, ruSS treadon,
daryL kLeiSt, PauL van deLSt, denniS keySer, john derber, MichaeL ek, jeSSe Meng, heLin Wei,
rongqian yang, StePhen Lord, huug va, and Mitch goLdberg jae-kyung ScheMM, WeSLey ebiSuzaki,
roger Lin, PingPing Xie, Mingyue chen, Shuntai zhou, Wayne higginS, cheng-zhi zou, quanhua Liu, yong
1350   chen, yong han, Lidia cucuruLL, richard W. reynoLdS, gLenn rutLedge, and A. 2010. "The NCEP Climate
Forecast System Reanalysis," no. August: 1015–58. https://doi.org/10.1175/2010BAMS3001.1.

Teuling, Adriaan J. 2018. "A Forest Evapotranspiration Paradox Investigated Using Lysimeter Data." *Vadose*
Zone Journal 17 (1): 170031. https://doi.org/10.2136/vzj2017.01.0031.

Theil, H. 1950. "A Rank-Invariant Method for Linear and Polynomial Regression." *I. II. III. Proceedings of the*
1355   *Section of Sciences*.

Tian, Feng, Jean Pierre Wigneron, Philippe Ciais, Jérôme Chave, Jérôme Ogée, Josep Peñuelas, Anders Ræbild,
et al. 2018. "Coupling of Ecosystem-Scale Plant Water Storage and Leaf Phenology Observed by
Satellite." *Nature Ecology and Evolution* 2 (9): 1428–35. https://doi.org/10.1038/s41559-018-0630-3.

Trajkovic, Slavisa. 2010. "Testing Hourly Reference Evapotranspiration Approaches Using Lysimeter
1360   Measurements in a Semiarid Climate," 38–49. https://doi.org/10.2166/nh.2010.015.

Trenberth, Kevin E., John T. Fasullo, and Jeffrey Kiehl. 2009. "Earth's Global Energy Budget." *Bulletin of the*

American Meteorological Society 90 (3): 311–23. https://doi.org/10.1175/2008BAMS2634.1.

Verstraeten, Willem W., Frank Veroustraete, and Jan Feyen. 2008. "Assessment of Evapotranspiration and Soil
Moisture Content across Different Scales of Observation." *Sensors* 8 (1): 70–117.
1365   https://doi.org/10.3390/s8010070.

Vinya, Royd, Yadvinder Malhi, Nick D Brown, Joshua B Fisher, Timothy Brodribb, and Luiz E O C Aragão.
2018. "Seasonal Changes in Plant – Water Relations in Fl Uence Patterns of Leaf Display in Miombo
Woodlands : Evidence of Water Conservative Strategies," no. Fuller 1999: 104–12.
https://doi.org/10.1093/treephys/tpy062.

1370   Wan, Z., Hook, S., Hulley, G. 2015. "MOD11A2 MODIS/Terra Land Surface Temperature/Emissivity 8-Day L3
Global 1km SIN Grid V006 [Data Set]." *NASA EOSDIS Land Processes DAAC*, no. April.
https://doi.org/https://doi.org/10.5067/MODIS/MOD11A2.006.

Wang-Erlandsson, Lan, Wim G.M. Bastiaanssen, Hongkai Gao, Jonas Jägermeyr, Gabriel B. Senay, Albert
I.J.M. Van Dijk, Juan P. Guerschman, Patrick W. Keys, Line J. Gordon, and Hubert H.G. Savenije. 2016.
1375   "Global Root Zone Storage Capacity from Satellite-Based Evaporation." *Hydrology and Earth System
Sciences* 20 (4): 1459–81. https://doi.org/10.5194/hess-20-1459-2016.

WaPOR Database Methodology. 2020. *WaPOR Database Methodology*. https://doi.org/10.4060/ca9894en.

WARMA. 2022. "Catchments for Zambia." Luangwa Catchment. 2022. http://www.warma.org.zm/catchments-
zambia/luangwa-catchment-2/.

1380   Weerasinghe, Imeshi, Wim Bastiaanssen, Marloes Mul, Li Jia, and Ann Van Griensven. 2020. "Can We Trust
Remote Sensing Evapotranspiration Products over Africa." *Hydrology and Earth System Sciences* 24 (3):
1565–86. https://doi.org/10.5194/hess-24-1565-2020.

White, F. 1984. *The Vegetation of Africa*. Paris: UNESCO.

World Bank. 2010. "A Multi-Sector Investment Opportunities Analysis." Washington, D.C.

1385   Zhang, Feng, Li Wen Zhang, Jing Jing Shi, and Jing Feng Huang. 2014. "Soil Moisture Monitoring Based on
Land Surface Temperature-Vegetation Index Space Derived from MODIS Data." *Pedosphere* 24 (4): 450–
60. https://doi.org/10.1016/S1002-0160(14)60031-X.

Zhang, Ke, John S. Kimball, and Steven W. Running. 2016. "A Review of Remote Sensing Based Actual
Evapotranspiration Estimation." *Wiley Interdisciplinary Reviews: Water* 3 (6): 834–53.
1390   https://doi.org/10.1002/wat2.1168.

Zhang, L., W. R. Dawes, and G. R. Walker. 2001. "Response of Mean Annual Evapotranspiration to Vegetation
Changes at Catchment Scale." *Water Resources Research* 37 (3): 701–8.
https://doi.org/10.1029/2000WR900325.

Zimba, Henry, Miriam Coenders-Gerrits, Banda Kawawa, Hubert Savenije, Imasiku Nyambe, and Hessel
1395   Winsemius. 2020. "Variations in Canopy Cover and Its Relationship with Canopy Water and Temperature

in the Miombo Woodland Based on Satellite Data." *Hydrology* 7 (3).
https://doi.org/10.3390/HYDROLOGY7030058.

Zimba, Henry; Coenders, Miriam; Savenije, Hubert H.G.; van de Giesen, Nick; Hulsman, Petra (2022):
ZAMSECUR Project Field Data Mpika, Zambia. 4TU.ResearchData. Dataset.
1400   https://doi.org/10.4121/19372352.v2